J Neurophysiol 98: 63–78, 2007.
First published May 16, 2007; doi:10.1152/jn.00152.2007.

Effects of Inhibitory Gain and Conductance Fluctuations in a Simple Model for Contrast-Invariant Orientation Tuning in Cat V1

Stephanie E. Palmer[1,2] and Kenneth D. Miller[1,3]

[1]*Department of Physiology and Sloan–Swartz Center for Theoretical Neurobiology, University of California at San Francisco, San Francisco, California;* [2]*Department of Physics and Lewis–Sigler Institute for Integrative Genomics, Carl Icahn Laboratory, Princeton University, Princeton, New Jersey; and* [3]*Center for Theoretical Neuroscience, Center for Neurobiology and Behavior, Columbia University Medical Center, New York State Psychiatric Institute Kolb Research Annex, New York, New York*

Submitted 9 February 2007; accepted in final form 10 May 2007

Palmer SE, Miller KD. Effects of inhibitory gain and conductance fluctuations in a simple model for contrast-invariant orientation tuning in cat V1. *J Neurophysiol* 98: 63–78, 2007. First published May 16, 2007; doi:10.1152/jn.00152.2007. The origin of orientation selectivity in primary visual cortex (V1) is a model problem for understanding cerebral cortical circuitry. A key constraint is that orientation tuning width is invariant under changes in stimulus contrast. We have previously shown that this can arise from the combination of feedforward lateral geniculate nucleus (LGN) input and an orientation-untuned component of feedforward inhibition that dominates excitation. However, these models did not include the large background voltage noise observed in vivo. Here, we include this noise and examine a simple model of cat V1 response. Constraining our simulations to fit physiological data, our single model parameter is the strength of feedforward inhibition relative to LGN excitation. With physiological noise, the contrast invariance of orientation tuning depends little on inhibition level, although very weak or very strong inhibition leads to weak broadening or sharpening, respectively, of tuning with contrast. For any inhibition level, an alternative measure of orientation tuning—the circular variance—decreases with contrast as observed experimentally. These results arise primarily because the voltage noise causes large inputs to be much more strongly amplified than small ones in evoking spiking responses, relatively suppressing responses to nonpreferred stimuli. However, inhibition comparable to or stronger than excitation appears necessary to suppress spiking responses to nonpreferred orientations to the extent seen in vivo and to allow the emergence of a tuned mean voltage response. These two response properties provide the strongest constraints on model details. Antiphase inhibition from inhibitory simple cells, and not just untuned inhibition from inhibitory complex cells, appears necessary to fully explain these aspects of cortical orientation tuning.

INTRODUCTION

The origin of orientation tuning in cat primary visual cortex (V1) has long served as a model problem for understanding how cerebral cortex transforms its inputs (e.g., Ferster and Miller 2000). In cats, orientation tuning is synthesized in layer 4, the input-recipient layer, which is dominated by simple cells, cells preferring light stimuli or dark stimuli in alternating, oriented bands of visual space (Martinez et al. 2005).

Simple cell responses to oriented stimuli are tuned for orientation and their tuning widths are invariant to changes in stimulus contrast (Alitto and Usrey 2004; Anderson et al. 2000a; Sclar and Freeman 1982; Skottun et al. 1987). The latter property provides an important constraint on mechanistic models of orientation tuning. Modeling shows that the summed feedforward input to a simple cell from the lateral geniculate nucleus (LGN) can be broken into two components: an orientation-tuned linear component that has contrast-invariant orientation tuning and a nonlinear component that is untuned—equal for all stimulus orientations—and grows with contrast (Troyer et al. 1998, 2002). In response to a drifting sinusoidal grating, the linear component is the first harmonic (F1) of the input, i.e., the size of its temporal modulation over a cycle, whereas the nonlinear component is dominated by the mean or DC of the input, i.e., the average input over a cycle (Fig. 1*A*). If the untuned DC of the LGN input were unopposed, it would cause an "iceberg" effect: a widening of orientation tuning with increasing stimulus contrast (Fig. 1*Ba*, *left*). We have argued that the DC LGN input can be suppressed and contrast-invariant tuning achieved by adding a component of feedforward inhibition (inhibition that is driven by LGN input, by cortical interneurons) that is untuned for orientation and grows with contrast (Lauritzen and Miller 2003; Troyer et al. 1998, 2002). Others have come to similar conclusions (McLaughlin et al. 2000; Wielaard et al. 2001). Some experimental support for such untuned inhibition now exists (Hirsch et al. 2003).

In our previous modeling work, significant voltage noise was not considered, except post hoc to smooth the input–output function in Troyer et al. (2002). Recent intracellular studies have found that, in response to a repeated stimulus, cat V1 layer 4 simple cells in vivo show large trial-to-trial voltage fluctuations, comparable in size to stimulus-locked voltage modulations (Anderson et al. 2000a). The trial-averaged voltage response largely remains subthreshold, so that spiking primarily occurs as the result of fluctuations from this average response (Anderson et al. 2000a).

Herein we address the effects of this voltage noise in a model of simple-cell orientation tuning. In the absence of noise, we had shown that, to achieve contrast-invariant tuning, feedforward inhibition must be stronger than feedforward LGN excitation (as in Fig. 1*Bc*, *left*; stronger as measured by the mean current when the cell is clamped at voltage threshold). This made the total untuned DC feedforward input negative, with size increasing with contrast. This compensated for growth of the input F1 with contrast that, if unopposed (as in Fig. 1*Bb*, *left*), would have provided suprathreshold input for

Address for reprint requests and other correspondence: S. E. Palmer, Lewis–Sigler Institute for Integrative Genomics, Carl Icahn Laboratory, Princeton University, Princeton, NJ 08544 (E-mail: sepalmer@princeton.edu).

The costs of publication of this article were defrayed in part by the payment of page charges. The article must therefore be hereby marked "*advertisement*" in accordance with 18 U.S.C. Section 1734 solely to indicate this fact.

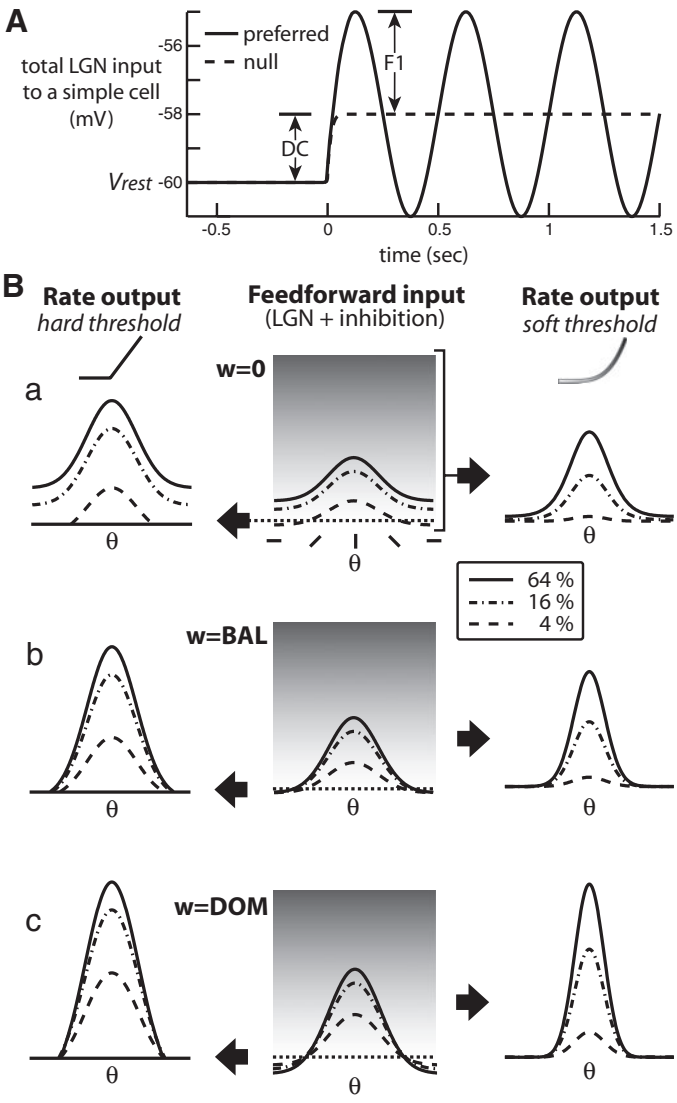

FIG. 1. Contrast invariance: an illustration of the problem. *A*: voltage induced by the lateral geniculate nucleus (LGN) input to a simple cell in primary visual cortex in response to a drifting sinusoidal luminance grating, without inhibition. This response can be broken into 2 components: the mean or average over a stimulus cycle, the direct current (DC); and the temporal modulation [or first harmonic (F1)]. F1 is tuned for orientation (largest at the preferred orientation and going to zero for nonpreferred orientations), whereas the DC is untuned, i.e., it is the same for all orientations. *B*, *middle column*: peak (F1 + DC) feedforward input to a simple cell as a function of stimulus orientation, for 3 stimulus contrasts (4, 16, and 64%) and 3 levels of inhibition (*a*: no inhibition, i.e., LGN input alone; *b*: inhibition that balances LGN excitation; *c*: strong inhibition that dominates LGN excitation). *Left* and *right columns*: effect of passing these inputs through a hard threshold or soft, power-law threshold (as induced by voltage noise), respectively. Note that with the hard threshold (*left column*), contrast-invariant orientation tuning [as measured by half-width at half-maximum (HWHM) response amplitude] arises only with dominant inhibition, whereas with a soft threshold, it appears to arise more flexibly. This paper explores this phenomenon. *Center column*: shading is meant to indicate the lift-off from zero of the power law. Dashed line indicates location of hard threshold for the *left column*. Curves in *center column* indicate peak input, i.e., F1 + DC. These can be decomposed as follows: the untuned DC is the "plateau" level on which a given curve sits, i.e., the value farthest from the preferred orientation, whereas the portion of the curve rising above this represents the tuned F1. In this figure, antiphase inhibition is assumed that subtracts from the LGN DC but adds to the LGN F1; other forms of inhibition that subtract from the DC without adding to the F1 are considered in the RESULTS.

more and more orientations as contrast increased. These opposing effects resulted in contrast-invariant tuning of the suprathreshold input (Troyer et al. 1998).

How does voltage noise alter this conclusion? The noise "smooths away" threshold, eliminating the sharp distinction between subthreshold and suprathreshold input, so that the relationship between trial-averaged voltage and spiking responses becomes a power-law function (Anderson et al. 2000a; Hansel and van Vreeswijk 2002; Miller and Troyer 2002) (Fig. 1*B*, *right column*). As a result, the theoretical requirement for contrast-invariant spiking responses is simply that the averaged voltage responses show contrast-invariant tuning (Hansel and van Vreeswijk 2002; Miller and Troyer 2002), as observed experimentally (Anderson et al. 2000a). What are the requirements on inhibition for this to occur? Must inhibition and excitation be precisely balanced to cancel the untuned input DC, leaving only the input F1, which has contrast-invariant tuning (as in Fig. 1*Bb*, *right*)? Would stronger or weaker inhibition disrupt the contrast invariance of tuning? Other questions also arise. How strong must inhibition be to account for the observed degree of suppression of voltage and spiking responses at nonpreferred orientations (Alitto and Usrey 2004; Anderson et al. 2000a)? What is required to account for the observed orientation-tuned, contrast-invariant DC voltage response to a drifting grating (Anderson et al. 2000a)? The DC component of the feedforward input is untuned, so a tuned DC component must be created in cortex from the cortical response to the tuned F1 input component, e.g., by recurrent excitation amplifying a tuned spiking response and/or by reversal potential effects that limit negative voltage excursions.

To address these questions, we study a minimal model: a pair of mutually excitatory simple cells, receiving both feedforward excitation from the LGN and untuned feedforward inhibition driven by LGN, in the presence of voltage fluctuations matched to those observed physiologically (Anderson et al. 2000a). We consider two models of inhibition, corresponding to two kinds of inhibitory cells observed in vivo in cat V1 layer 4 (Hirsch et al. 2003): *1*) inhibitory simple cells with an orientation-untuned component to their response and providing antiphase inhibition (as in Troyer et al. 1998) and *2*) inhibitory complex cells that are untuned for orientation (as in Lauritzen and Miller 2003). We explore this model parametrically and determine the strength of inhibition required to yield the response properties described earlier. Although the model is simplified, our study of it reveals key issues and trade-offs required to account, more generally, for these response properties.

METHODS

Analysis of experimental data

We analyzed raw voltage traces graciously provided to us by J. Anderson and D. Ferster from their intracellular in vivo recordings in cat V1 reported in Anderson et al. (2000a). These data are for five simple cells and were collected at three contrasts and several orientations for drifting grating stimuli with a 2-Hz temporal frequency.

For these cells, we averaged quantities such as firing rate and mean voltage across trials at each orientation and contrast. In all analyses of voltage, spikes were first detected by high-pass filtering and then replaced by their threshold voltage. We analyzed the mean and modulation of the voltage by examining the components of the

Fourier transform at zero frequency (the mean or DC component) and at the frequency of the grating stimuli, 2 Hz (the first harmonic or F1 component). Details of the voltage fluctuations were analyzed by subtracting the mean voltage from each trial and binning the remaining voltage fluctuations. Two-time correlation functions in the background voltage fluctuations were obtained by removing spikes and subtracting the mean from each trial, putting all trials together in one voltage trace, and computing the autocorrelation.

Rate and voltage orientation tuning curves were obtained by fitting the data $y(\theta)$ to a Gaussian curve plus a baseline $A \exp[-(\theta-\theta_0)^2/2\sigma^2] + B$, where the goodness of fit of the full function versus the mean B alone was assessed using an F-test. If the P-value from this test was >0.05, we fit the data to B alone and assign the width a value of 90°, which we classify as flat. We measure the widths of these tuning curves using a variety of measures. One measure is the σ from the Gaussian fit. Another is the half-width-at-half-maximum (HWHM) of the tuning curve, measured relative to the background firing rate or the resting membrane potential. We also calculated the circular variance for each tuning curve.

We use the slope of these width quantities, as a function of $\log_{10}$ (*contrast*), to assess contrast invariance. In the Anderson–Ferster data, three nonzero contrasts were tested: 8 or 12, 20, and 64%. The slope is calculated over these three contrasts. To obtain an estimate of the variance of these derived quantities, we perform a bootstrap resampling of the data.

Model overview

We simulate the responses of simple cells in layer 4 of cat V1 to drifting grating stimuli. We simulate two simple cells with identical receptive fields that excite one another (recurrent excitation). The simple cells receive feedforward input from the lateral geniculate nucleus (LGN), feedforward inhibition from cortical inhibitory cells driven by LGN input, and noise input that simulates voltage fluctuations observed in vivo in such cells.

We model responses to drifting grating stimuli characterized by an orientation θ; a spatial frequency f_{stim}, which we take to be constant and equal to the frequency f_{RF} of the Gabor function describing the simple cell receptive fields (subsequently described); $f_{stim} = f_{RF} = 0.8$ cycles/deg; a temporal frequency $\omega = 2$ Hz; and a contrast C.

LGN input

We model the LGN component of the feedforward input to the simple cells as in Troyer et al. (2002). Each simple cell has a receptive field defined by a Gabor function, $G(x)$, of even phase, where the vector x defines the coordinates in the two-dimensional (2-D) plane. The preferred spatial frequency of the Gabor, $f_{RF} = 0.8$ cycles/deg, is a typical value for about 5° eccentricity in the cat (Movshon et al. 1978). The parameters of the Gabor are the same as the "broadly tuned" parameters of Troyer et al. (1998).

We define the positive and negative parts of the Gabor as G^+ and G^-, respectively: $G^+(x) = \max\{G(x), 0\}$ and $G^-(x) = \max\{-G(x), 0\}$. Then, assuming that positive (negative) parts of the Gabor receive ON-center (OFF-center) LGN input, assuming a linear model of the LGN input, and ignoring the discrete nature of the grid of LGN cells, the total LGN input to the simple cell may be written as

$$I_{LGN}(t) = \int d\mathbf{x} G^+(\mathbf{x}) L^{ON}(\mathbf{x}, t) + G^-(\mathbf{x}) L^{OFF}(\mathbf{x}, t) \quad (1)$$

where $L^{ON}(\mathbf{x}, t)$, $L^{OFF}(\mathbf{x}, t)$ describe the response of an LGN ON- or OFF-center cell, respectively, centered at spatial position $\mathbf{x}$ to a time-varying sinusoidal grating stimulus.

We assume that the LGN inputs respond almost linearly to a sinusoidal grating, in that they show a sinusoidal modulation of firing rate in response to the sinusoidal stimulus. However, there are two nonlinear aspects of response. First, the firing-rate modulation is rectified, meaning that rates cannot drop below zero. Second, the amplitude of the modulation is a nonlinear function of contrast, of the form $R_{max}C^n/(C_{50}^n + C^n)$. We define the 2-D vector $\mathbf{f}_{stim}$ that describes both the orientation and spatial frequency of the grating stimulus $|\mathbf{f}_{stim}| = f_{stim}$, and the angle of $\mathbf{f}_{stim}$ is orthogonal to θ. Thus the $L(\mathbf{x}, t)$ values in response to the grating stimulus are given by

$$L^J(\mathbf{x}, t) = \left[R^J_{max} \frac{C^{n^J}}{C_{50}^{n^J} + C^{n^J}} \cos(2\pi \mathbf{f}_{stim} \cdot \mathbf{x} - 2\pi\omega t + \phi^J) + R^J_{bkgnd} \right]^+$$

where $[x]^+ = x$; $x \geq 0$ and $[x]^+ = 0$; $x < 0$. Here, J takes the values ON or OFF. The phases are given by $\phi^{ON} = 0$, $\phi^{OFF} = \pi$; that is, we assume that the OFF cell at a given spatial position responds with the opposite temporal phase (a shift of 180°) as the ON cell at the same spatial position. Following Troyer et al. (1998) and Cheng et al. (1995), the other parameters are given by: $R^{ON}_{max} = 53$ Hz, $n^{ON} = 1.20$, $C^{ON}_{50} = 13.3\%$, $R^{ON}_{bkgnd} = 10$ Hz, $R^{OFF}_{max} = 48.6$ Hz, $C^{OFF}_{50} = 7.18\%$, and $R^{OFF}_{bkgnd} = 15$ Hz.

Define the function $|G|$ as the absolute value of the Gabor: $|G|(\mathbf{x}) = |G(\mathbf{x})|$. If we note that $G(\mathbf{x}) = G^+(\mathbf{x}) - G^-(\mathbf{x})$, whereas $|G|(\mathbf{x}) = G^+(\mathbf{x}) + G^-(\mathbf{x})$, and we define $L_{avg} = (L^{ON} + L^{OFF})/2$ and $Ldiff = (L^{ON} - L^{OFF})/2$, we can rewrite *Eq. 1* for $I_{LGN}(t)$ as

$$I_{LGN}(t) = \int d\mathbf{x} G(\mathbf{x}) L_{diff}(\mathbf{x}, t) + |G|(\mathbf{x}) L_{avg}(\mathbf{x}, t)$$

Troyer et al. (2002) showed that the spatial Fourier transform of this input was dominated by two components: a DC or time-independent component that depends only on stimulus contrast and an F1 component (time-varying sinusoidally, with the frequency of the stimulus) that depends on both stimulus contrast C and stimulus orientation θ. In particular, the total LGN input can be written

$$I_{LGN}(t) \cong DC(C) + F1(C, \theta) \cos(2\pi\omega t) \quad (2)$$

where

$$DC(C) = |\mathcal{G}|^0 a^0_{avg}(C)/[\mathcal{G}^1(0) a^1_{diff}(100\%)]$$

$$F1(C, \theta) = \mathcal{G}^1(\theta) a^1_{diff}(C)/[\mathcal{G}^1(0) a^1_{diff}(100\%)]$$

The a_{avg} and a_{diff} terms represent a spatial Fourier transform of the average $L_{avg}(\mathbf{x})$ and difference $L_{diff}(\mathbf{x})$, respectively, of the responses of LGN ON-center and OFF-center cells. The superscript reflects the harmonic of the spatial frequency $\mathbf{f}_{stim}$ of the grating at which these amplitudes are measured. The variable θ represents the orientation of the stimulus and thus the orientation at which the spatial 2-D Fourier transform is measured, where $\theta = 0$ is the preferred orientation of the cell. The $\mathcal{G}$ and $|\mathcal{G}|$ terms are the Fourier transform of the Gabor receptive field and the Fourier transform of the absolute value of the Gabor, respectively, and are also taken at multiples of $\mathbf{f}_{stim}$ because these components dominate the expansion. The resulting DC and F1 terms contain a contrast dependency inherited from the LGN cells $[a_{avg}(C), a_{diff}(C)]$ and an orientation dependency from the Gabor $[\mathcal{G}(\theta)]$. They are normalized so that the response to the optimal stimulus at maximal contrast gives an F1 amplitude of 1. The DC amplitude at maximal contrast is then 0.87.

We take the total LGN input to a simple cell to be given by *Eq. 2* but with negative values set to zero

$$I_{LGN}(t) = [DC(C) + F1(C, \theta) \cos(2\pi\omega t)]^+ \quad (3)$$

We use a conductance-based integrate-and-fire model to simulate our cortical simple cells. We take the excitatory conductance opened by the LGN input to be proportional to $I_{LGN}(t)$ as given by *Eq. 3*. For the case of simple-cell inhibition, we assume that feedforward inhibition comes from simple cells receiving identical LGN input except with opposite temporal phase. The inhibitory input to the excitatory cell is assumed to be linear in this LGN input, but scaled by an overall

inhibitory gain factor w, which gives the relative strength of the inhibitory versus excitatory input. Thus the total feedforward (FF) input to the simple cell becomes

$$I_{FF} = g^E_{LGN}(V_E - V) + g^I_{FF}(V_I - V) \quad (4)$$

where

$$g^E_{LGN} = g_{stim}[DC(C) + F1(C, \theta) \cos(2\pi\omega t)]^+$$

and

$$g^I_{FF} = w g_{stim}[DC(C) - F1(C, \theta) \cos(2\pi\omega t)]^+$$

The excitatory conductance has a reversal potential $V_E = 0$ mV and inhibition $V_I = -70$ mV. We also consider inhibition from a complex-cell–like source, in which case $g^I_{FF,complex} = w g_{stim} DC(C)$.

The stimulus amplitude g_{stim} is adjusted so that the cells have a range of modulations of the voltage responses to drifting gratings that approximately matches the range observed in vivo, which effectively sets our contrast scale. In the full model, which includes recurrent excitation (subsequently described), setting $g_{stim} = 2.0$ nS gives a 3.0- to 4.4-mV range of voltage modulation and a 0.4- to 1.3-mV range of voltage mean at the preferred orientation of the cell in a contrast range of 8 to 64% for $w = 2.5$. In the model with complex-cell inhibition, the inhibition does not add to the F1, so we adjust g_{stim} to compensate. By setting $g_{stim} = 4.0$ nS (other parameters set as subsequently described), we obtain an F1 range of 3.6 to 4.8 mV and a DC range of 0.3 to 1.4 mV over the same contrasts and at $w = 2.5$.

Noise

Noise in the model is generated by an Ornstein–Uhlenbeck process as in Destexhe et al. (2001), with parameters set to match the voltage fluctuations observed in these cells. There are several independent noise processes that contribute to the conductances, as subsequently described. Calling any one such process $\eta(t)$, it is determined by the equation

$$d\eta(t) = -\kappa\eta(t)dt + \sqrt{D}dW(t)$$

which is the Ornstein–Uhlenbeck process. The term $-\kappa\eta(t)$ represents drift back to zero with characteristic timescale $1/\kappa$. The other term is the Weiner process: D is the diffusion constant and $dW(t)$ denotes a Gaussian white noise process. It has been shown previously (Destexhe et al. 2001; Gillespie 1996) that this process has an exact update rule that allows a simple approach to integrating the differential equations for the conductances. The update rule is

$$\eta(t + \Delta t) = e^{-\kappa\Delta t}\eta(t) + \sqrt{\frac{D}{2\kappa}(1 - e^{-2\kappa\Delta t})}\, N(0, 1) \quad (5)$$

where $N(0, 1)$ is a random number drawn from a Gaussian distribution with mean zero and unit SD.

We inject independent conductance fluctuations in the excitatory and in each of two inhibitory channels. The noise in each conductance is characterized by a constant mean level g_{bkgnd} and the time-varying noise $\eta(t)$. Because the noise cannot inject a negative conductance, the sum of these two terms is rectified at zero. Thus the expressions for the excitatory and inhibitory conductances can be written as

$$g^X_{noise} = [g^X_{bkgnd} + \eta^X(t)]^+ \quad (6)$$

where $X = E$, I_a, or I_b. We have introduced two inhibitory noise processes, I_a and I_b, with reversal potentials of -70 and -90 mV, respectively. We think of these roughly as corresponding to γ-aminobutyric acid types A and B ($GABA_A$ and $GABA_B$, respectively) conductances, respectively. More generally, we expect that real cells would have fluctuating input from many types of channels with different reversal potentials. The preceding choice gives one noise process per reversal potential we use in the model because we have a 0-mV excitatory channel, a -70-mV inhibitory channel from the LGN input, and a -90-mV channel from the adaptation current (see following text). Furthermore, the -90-mV noise processes appeared needed to match the data. Using only a single inhibitory noise process with reversal potential -70 mV, it was difficult to get the width of the distribution of voltage fluctuation amplitudes to be as wide as observed experimentally without driving the background firing rate up (i.e., without having too many fluctuations toward suprathreshold voltages). Adding a second process with reversal potential -90 mV allowed the distribution to widen away from threshold, so that we could obtain both realistic distribution widths and realistic background firing rates.

The parameters of the noise processes were set as follows: All were constrained to have the same time constant $1/\kappa$. Its value was determined by a fit to the autocorrelation in voltage fluctuations as observed intracellularly by Anderson and Ferster in cat V1 simple cells. Here we assume that the correlation time in the voltage fluctuations corresponds to the sum of the characteristic time in the conductance fluctuations and the membrane time constant. The two-time correlation function for an Ornstein–Uhlenbeck process may be written as (Gillespie 1996)

$$\langle \eta(t_1)\eta(t_2) \rangle = \frac{D}{2\kappa} e^{-\kappa|t_1 - t_2|}$$

We fit this autocorrelation to a single exponential. As shown in Fig. 2, this gives a correlation time of approximately 29 ms at background (stimulus contrast of 0%). Given a cell time constant of 15 ms at rest, we use $1/\kappa = 29 - 15 = 14$ ms in all of our noise processes. This yields a good match between correlation times in model and experimental voltage fluctuations (Fig. 2).

We set the mean amplitudes of the two inhibitory noises equal because we have no reason to think one or the other dominates. To mimic the width of the voltage fluctuations about rest seen in vivo of 3.47 ± 0.42 mV (SD given across the five cells we chose for our analysis) and to maintain a background firing rate that is nonzero but not $\gtrsim$1 Hz, we set $g^E_{bkgnd} = 6.5$ nS, $g^{Ia}_{bkgnd} = g^{Ib}_{bkgnd} = 9.0$ nS, $D^E = 0.67$ nS^2/ms, and $D^{Ia} = D^{Ib} = 1.29$ nS^2/ms. With these parameters we are able to obtain SD = 3.50 mV in our voltage fluctuations in the model.

Recurrent excitation

We seek to mimic excitation from similarly tuned cells in the network (recurrent excitation), yet keep the model as simple as possible. As a first and minimal pass at reproducing recurrent excitation, we add a single additional simple cell with the same receptive field as the first cell and connect the two with reciprocal excitatory synapses. The two cells receive identical stimulus-dependent excitation and inhibition from the LGN and receive noise that is statistically identical (governed by the same parameters) but independent. The recurrent synapse is assumed to be a mixture of *N*-methyl-D-aspartate (NMDA) and α-amino-3-hydroxy-5-methyl-4-isoxazolepropionic acid–receptor-mediated currents and is defined as

$$g_{recurrent}(t) = g_{rec\_amp} \sum_i 0.8\{A^{fast}_{NMDA} \exp[-(t - \tilde{t}_i)/\tau^{fast,fall}_{NMDA}] + A^{slow}_{NMDA} \exp[-(t - \tilde{t}_i)/\tau^{slow,fall}_{NMDA}] - \exp[-(t - \tilde{t}_i)/\tau^{rise}_{NMDA}]\} + 0.2\{\exp[-(t - \tilde{t}_i)/\tau^{fall}_{AMPA}] - \exp[-(t - \tilde{t}_i)/\tau^{rise}_{AMPA}]\} \quad (7)$$

where $A^{fast}_{NMDA} = 0.88$, $A^{slow}_{NMDA} = 0.12$, $\tau^{fast,fall}_{NMDA} = 63.0$ ms, $\tau^{slow,fall}_{NMDA} = 200.0$ ms, $\tau^{rise}_{NMDA} = 5.5$ ms, $\tau^{fall}_{AMPA} = 4.0$ ms, and $\tau^{rise}_{AMPA} = 0.2$ ms, as in Krukowski and Miller (2001) but with an altered τ^{fall}_{AMPA} chosen to agree more closely with in vitro data from rat cortex (Hausser and Roth 1997; Hestrin 1993; Hestrin et al. 1990; Stern et al. 1992). The sum is over all previous spike times $\langle t_i \rangle$, where $\tilde{t}_i = t_i + t_d$ imposes a

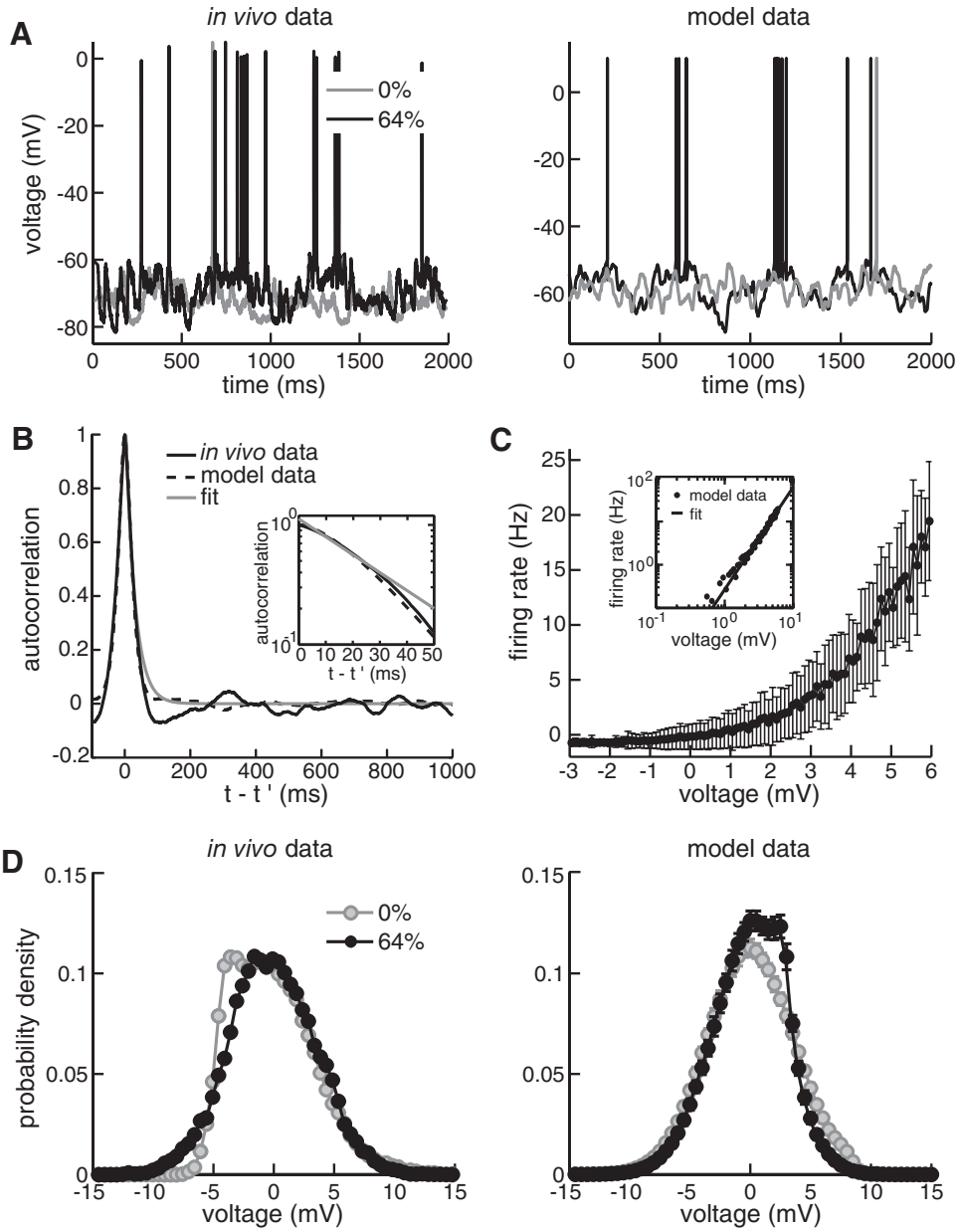

FIG. 2. Comparison of voltage fluctuations in our model data to in vivo intracellular data. *A*: example traces of single-trial responses to drifting grating stimuli at the preferred orientation of the cell at 0% contrast (background), marked with gray lines, and 64% contrast, black lines. Intracellular data are shown on the *left* and model data are shown on the *right*. *B*: autocorrelation in the background fluctuations of the voltage in the in vivo data, shown in black, is fit to a single exponential, which was used to define the time constant of the model noise processes. Fit is shown in gray; the resulting autocorrelation in the model data voltage fluctuations is shown with a dashed line. *C*: input–output curve for the model cell. Average voltage was calculated over 20-ms increments and binned in 0.1-mV increments for each value of the inhibitory gain w. Firing rate was calculated within the same time bin and the background rate was subtracted. Data here are plotted for $w = 2.5$. Error bars show SDs of the rate in each voltage bin. *Inset*: same data on a log–log plot along with a fit to the function $rate = cV^{\alpha}$, which gives $\alpha = 2.36$. *D*: histograms showing probability density distributions for voltage fluctuations around the trial-averaged mean response. On the *right*, for the model data, the mean distributions are shown as well as the SD in each voltage bin. Black bars represent 64% contrast and gray bars represent background fluctuations.

synaptic delay, $t_d = 1.5$ ms, between spiking in one cell and the arrival of that impulse at the other. For simplicity, and because this conductance is activated only when the voltage is near spike threshold, the voltage dependency of the NMDA conductance is ignored. To obtain firing rates at $\theta = 0$ and 100% contrast between 5 and 15 Hz for the w values chosen here, we set $g_{rec\_amp} = 4.5$ nS. At $\gtrsim$6 nS, the rate enters a nonphysiologic positive feedback regime, whereas at $\lesssim$1 nS, we do not see much effect of the recurrence.

Spiking

We set the threshold voltage about 10 mV above rest, to mimic approximately the relationship between rest and threshold seen in real V1 simple cells. When the cell's voltage reaches spike threshold, $V_{thresh} = -50$ mV, a spike occurs, and after an absolute refractory period of 1.5 ms the cell's voltage is reset to $V_{reset} = -56$ mV. The reset voltage is set so that the slope of the firing rate versus the size of a constant injected input current (*f–I*) curve matches that seen in slice experiments, as in Troyer and Miller (1997). For this analysis, we set the noise, recurrent, LGN, and feedforward connection strengths to zero. With a $V_{reset} = V_{thresh} - 6$ mV $= -56$ mV, we obtain a slope of 235.9 Hz/nA, which agrees well with the average slope measured in slice by McCormick and colleagues, 241 Hz/nA. After each spike, we open a spike rate adaptation conductance that takes the form

$$g_{adpt}(t) = g_{adpt\_amp} \sum_i \exp[(t - t_i)/\tau_{rise}] - \exp[(t - t_i)/\tau_{fall}] \quad (8)$$

with $g_{adpt\_amp} = 3.0$ nS, $\tau_{rise} = 1.0$ ms, and $\tau_{fall} = 83.3$ ms, as in Troyer et al. (1998). The sum is over all previous spike times $\langle t_i \rangle$. The reversal potential of this conductance is -90 mV.

dV/dt for a simple cell in our model

By combining these conductances and one more to be subsequently described, we obtain the main equation we use in simulating responses of our model neurons to input stimuli

$$C\mathrm{d}V(t)/\mathrm{d}t = (g^{E}_{LGN} + g_{recurrent} + g^{E}_{noise})[V_E - V(t)] + (g^{I}_{FF} + g^{Ia}_{bkgnd,offset} + g^{Ia}_{noise})[V_{Ia} - V(t)] + (g^{Ib}_{noise} + g_{adpt})[V_{Ib} - V(t)] \quad (9)$$

where $C = \tau_{cell}/R_{input}$. At rest, the input resistance of our cell is 31.75 MΩ and $\tau_{cell} = 15$ ms. This gives a capacitance $C = 0.472$ nF. At the maximally driving stimulus, the input resistance drops to 15.36 MΩ, leading to a conductance ratio between maximal stimulus and background of about 2, which agrees with experiment (e.g., Anderson et al. 2000b; Monier et al. 2003).

LGN cells have nonzero background firing rates, so that $g^{I}_{FF} \cong 0.5wg_{stim}$ at 0% contrast. As w increases, this contribution to the inhibitory conductance also increases. To maintain a constant background conductance state for each value of w, we need to balance the background input from the feedforward responses by offsetting the inhibitory DC term. We do this by starting from a large w state, $w_l = 6.0$, and adding to the background whatever DC inhibition is needed to keep background inhibition constant as w changes

$$g^{Ia}_{bkgnd,offset} = (w_1 - w)(0.5g_{stim})$$

Integration algorithm

We implement this scheme for modeling the membrane potential of the cell using a time step of 0.25 ms in the model and updating according to

$$V(t + \Delta t) = V(t)e^{-\Delta t/RC_{cell}} + V_{SS}(1 - e^{-\Delta t/RC_{cell}})$$

where $R = \sum_n g_n$ is the instantaneous resistance of the cell at time t and C_{cell} is the capacitance of the cell. The term V_{SS} is the steady-state voltage, given by

$$V_{SS} = R \sum_n g_n V_n$$

where the sum over n runs over all our conductances and their corresponding reversal potentials. For our model, we have found that this integrator behaves as well as one using a fourth-order Runge–Kutta algorithm, differing from the latter only by ±0.001 mV root mean square (RMS). All simulations of a given stimulus are run for 3 s. We presented stimuli at 10 contrasts (0, 0.5, 1, 2, 4, 8, 16, 32, 64, and 100%) and 11 orientations (0, 5, 10, 15, 20, 25, 30, 40, 50, 70, and 90°). We have no direction dependency in the model, so without loss of generality we can consider only positive orientations. Tuning curves are plotted symmetrically for visualization purposes. We perform 1,000 trials of each stimulus and group these trials into 50 "experiments" of 20 trials each.

Tuning fits and measures

We use the same tuning fits and width measures for our model data as we described in characterizing the experimental data from Anderson and Ferster. The σ, HWHM, and circular variance were calculated for each w and contrast. The slopes of these fits were calculated over all contrasts and also only at contrasts where reliable tuning was measured at every value of w (≥4%, for example). Because we have access to a large number of trials, we calculate variance in derived quantities directly by using several sets of independent "experiments." Specifically, we have 50 "experiments" each consisting of data from 20 trials taken at each orientation, contrast, and w. The 50 "experiments" allow us to obtain error bars on tuning widths and quantities we derive using these widths, such as the slope of the widths over contrast. We also performed the same analyses using 10, 50, and 100 trials per stimulus. We found that the 20-trial averaged data were the best compromise between finding fits that matched our best estimate of the actual mean tuning in the model, which we approximate by examining the 1,000-trial averaged tuning, and comparing our model data to the number of trials realistically achievable in an in vivo experiment.

Other parameter sets

We also tested a model with complex-cell–like feedforward inhibition, in which $g^{I}_{FF} = g^{I}_{FF,complex} = wg_{stim}DC(C)$. Because the F1 of the LGN input is not amplified by the inhibitory gain, we raise the stimulus conductance and adjust the total background inhibitory conductances accordingly to maintain the same range of modulations in the membrane potential with the stimulus frequency. For these simulations, we set $g_{stim} = 4.0$ nS, $g^{Ia}_{bkgnd} = 5.0$ nS, $g^{Ib}_{bkgnd} = 9.0$ nS, $D^{Ia} = 0.40$ nS^2/ms, and $D^{Ib} = 1.29$ nS^2/ms. We lowered the I_a background conductance to offset the introduction of a higher feedforward background inhibition resulting from the increase in g_{stim}. We increased the I_b conductance slightly to keep firing at rest <1 Hz. All other parameters remained the same and the cell's input resistance at rest is 29.00 MΩ. The SD of the voltage noise is about the same, here being 3.14 mV. With this parameter set, as stated earlier, the F1 varies over 3.5 to 4.9 mV and the DC over −0.2 to 3.4 mV between 8 and 64% contrast and over the full w-range.

Unless otherwise noted, error bars in plots of model data show the SE across the 50 "experiments" we performed with 20 trials each.

RESULTS

Basic model

Our model addresses the effects of noise on the amount of inhibitory gain required to obtain contrast-invariant orientation tuning in V1 simple cells. By constraining all but one parameter—the strength of inhibition—we are able to discuss cleanly the effects of noise and assess how inhibition affects the width of orientation tuning. We use a conductance-based single-compartment integrate-and-fire cell model. To qualitatively include the effects of recurrent intracortical excitation while keeping the model as simple as possible, we include two simple cells that mutually excite one another.

We study responses to drifting grating stimuli filtered through a simple model of the lateral geniculate nucleus (LGN). As was shown previously (Troyer et al. 2002), the total input to a simple cell from the LGN in response to such a periodic stimulus can be written as a constant (DC) term, plus a term that temporally modulates with the temporal frequency of the grating (F1) (Fig. 1*A*). Both terms inherit their contrast response properties from the ON and OFF cells in the LGN. For a given stimulus contrast C, the size of the F1, but not of the DC, depends on the orientation of the drifting grating θ. The excitatory conductance from the LGN can thus be written as

$$g_{LGN} = g_{stim}[DC(C) + F1(C, \theta)\cos(2\pi\omega t)]^{+}$$

where g_{stim} determines the overall amplitude of this conductance and $[x]^{+} = \max\{x, 0\}$. The F1 and DC terms are normalized such that at the preferred orientation of the cell and maximal contrast, F1 = 1. We take this as the excitatory input to our simple cells.

With only this form of stimulus-induced input, orientation tuning width would grow with increasing contrast (Fig. 1*Ba*). To kill this so-called iceberg effect, something must suppress the untuned DC response. A relative suppression is achieved by the power-law input–output relationship that is induced by the voltage noise, discussed in the following text, because this amplifies larger inputs much more than smaller ones (Fig. 1*Bb*, *right column*). However, additional suppression may be required, as we explore here. We consider two possible sources for such suppression: antiphase inhibition from similarly tuned

simple cells (see *Eq. 4*) and complex-cell–like inhibition. We present detailed results for simple cell inhibition and then summarize results for complex-cell inhibition.

Our main results involve the examination of contrast invariance of various measures of orientation tuning, of both the spiking and the voltage responses, as a function of the weight of the inhibition, which is governed in our model by the parameter w. Because of the difference in reversal potentials of excitatory and inhibitory stimulus-driven conductances (0 and −70 mV, respectively), stimulus-induced excitatory and inhibitory currents are balanced at threshold voltage (−50 mV) when $w = 2.5$. We will refer to $w = 2.5$ as "balanced inhibition" and to significantly larger values of w as "strong inhibition" and significantly smaller values as "weak inhibition."

Voltage fluctuations

Our model is constrained to reproduce the sorts of background voltage fluctuations observed in vivo. The cells are each given three independent background noise conductance inputs, one representing an excitatory conductance with reversal potential 0 mV and one each representing inhibitory conductance with reversal potentials of −70 and −90 mV, respectively. Noise processes between the two cells are not correlated. We assume that each noise conductance can be modeled as a random walk with a drift back to a mean value as described by *Eq. 5*. The parameters describing the noise are fit so that the background firing rate of the cells is ≲1 Hz, and the resulting voltage noise fluctuations match those seen in experimental data from cat V1 cells (provided by Anderson and Ferster).

The resulting voltage traces at rest and in response to a grating at the preferred orientation and 64% contrast show similar voltage fluctuations in a model cell with $w = 2.5$ as in a simple cell in cat V1 recorded in vivo (Fig. 2, *A* and *B*). This can be examined more precisely by plotting a histogram of the fluctuations about the mean background potential (Fig. 2*D*), from which it can be seen that the distribution of voltage fluctuations in the model reasonably matches that observed in vivo. There are also some small differences: the particular cell illustrated in Fig. 2*D* shows a slightly non-Gaussian behavior, having what may be a second peak at a slightly negative potential relative to rest. Other cells did not show this behavior, so we did not attempt to reproduce this possible two-state switching. Across the five cat V1 cells we analyzed, the width of the background voltage fluctuations was 3.47 ± 0.42 mV. The width of the model voltage noise distribution at rest was 3.5 mV and was constant over all values of w tested.

As a result of the voltage noise, the relationship between the trial-averaged rate r and the trial-averaged voltage V is well described by a power law $r \propto V^{\alpha}$, where the membrane potential is measured relative to the mean resting membrane potential (and excursions below rest are set to zero) and rate is measured with mean background firing subtracted (see Fig. 2*C*, for the case $w = 2.5$) (Hansel and van Vreeswijk 2002; Miller and Troyer 2002). We fit this curve to the function $R = cV^{\alpha}$ with a least-squares procedure over a voltage range from 0.01 mV to the maximum voltage observed for that particular w. We find that the power α falls in the range $2.16 \leq \alpha \leq 3.19$ over the set of w values we tested, and roughly increases with w. These values are comparable to, although a bit less than, those observed in vivo, where the most common values are in the range 2.75–3.5 (Priebe et al. 2004).

Rate and voltage tuning curves

In response to a drifting grating stimulus, the orientation-tuning curves for the firing rate show an untuned component that grows with contrast for very weak inhibition, but that is largely or entirely eliminated by balanced or strong inhibition (Fig. 3). Contrast invariance can be assessed by eye in these plots by examining the overlap of the rescaled curves plotted to the *right* of each set of raw data. Only moderate inhibition (inhibition greater than $w = 0.5$ but less than the balanced level, $w = 2.5$) is needed to bring the major parts of the scaled curves, excluding the tails, into alignment. Increasing inhibition brings the tails of the scaled rate curves into alignment and then leads to suppression of the tails of the scaled high-contrast curves relative to those of the low-contrast curves. The tuning curves for peak voltage behave similarly but seem to require somewhat more inhibition for a given behavior than the rate

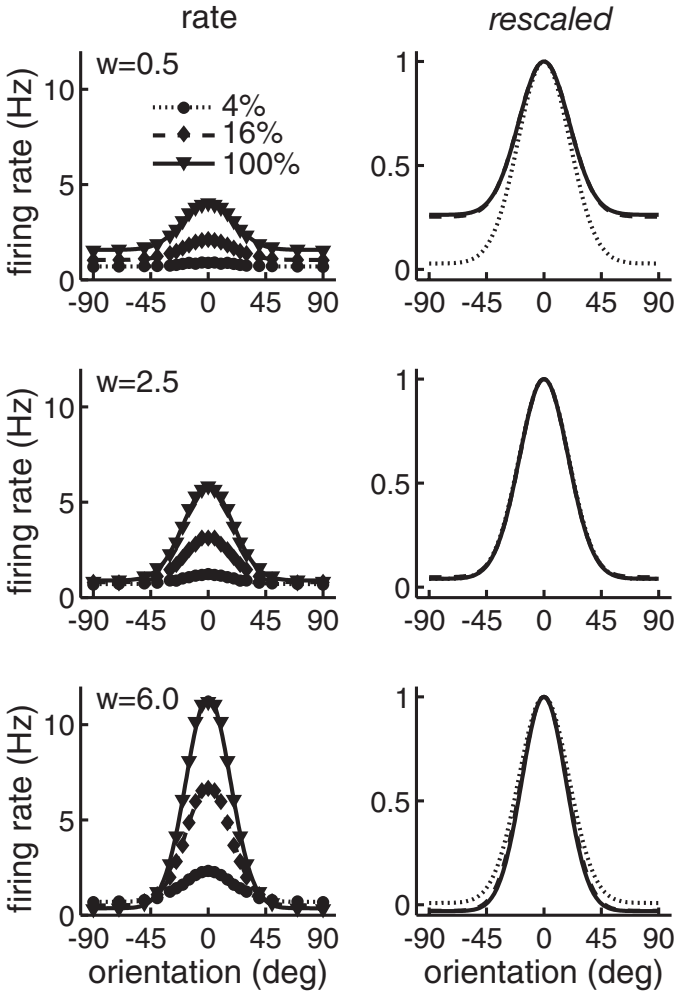

FIG. 3. Rate tuning curves for our model cell as a function of orientation. Rate is shown at 3 contrasts (4, 16, and 100%) and is plotted for each of 3 values of w ($w = 0.5$, 2.5, and 6.0 from *top* to *bottom*). On the *left*, the symbols plot mean and SE responses, whereas the lines correspond to best fit of a Gaussian plus a baseline. Error bars indicate SE and are smaller than the symbols used here to plot the mean. On the *right*, curves are normalized so that peaks coincide at 1 and 0 marks the background firing rate.

curves (data not shown). This difference coupled with the fact that the peak voltage curves are more broadly tuned than the rate curves are expected, given the power-law relation between voltage and rate, which amplifies large voltage responses much more than small ones.

The basis for this tuning can be better understood by separately examining the F1 and DC of the voltage response (Fig. 4). The voltage F1 shows contrast-invariant tuning at all inhibition levels (Fig. 4*B*), as expected, because the F1 of the LGN input shows contrast-invariant tuning. The problem in creating contrast-invariant spiking orientation tuning is presented by the voltage DC, which is constant across orientations for the LGN input. This untuned DC input component must be sufficiently suppressed so that, even at high contrast, it does not by itself drive significant spiking, as assessed by the spiking response at orientations far from the preferred. In our model, this requires moderate inhibition (Fig. 4*A*; compare with Fig. 3*A*). Furthermore, to match experiments, the voltage DC itself should show contrast-invariant orientation tuning. This requires that a tuned voltage DC component be created. In our model, this is created by recurrent excitation, which increases net depolarization to stimuli that induce spiking. This also requires that the untuned DC component be sufficiently suppressed that the tuned DC component dominates it, which requires strong inhibition in our model (Fig. 4*A*).

Contrast invariance of tuning

As can be seen in Figs. 3 and 4, the degree to which tuning curves are judged to be contrast invariant depends on which aspects of the curves are examined. We consider several measures that are commonly used in the literature and that assess different aspects of tuning. First, we consider the SD, or σ, of the Gaussian when the curves are fit by the sum of a Gaussian and a flat background term. This measure is insensitive to an untuned component of response or to the level of response to nonpreferred orientations because this is captured by the background term. Thus it captures only the width of the tuned part of the curve. Second, we consider the half-width at half-maximum (HWHM) of the tuning curve, where the size of the maximum response is measured relative to background firing rate or resting membrane potential (not relative to the response to nonpreferred orientations). This measure is sensitive to responses that are half the maximum response or larger and so becomes sensitive to an untuned component of response when such a component has a size comparable to the half-maximum. Finally, we consider the circular variance of the tuning curve, a measure that is strongly affected by the size of the response to nonpreferred orientations relative to the preferred. In experimental studies, HWHM and σ show contrast invariance (Alitto and Usrey 2004; Anderson et al. 2000a; Sclar and Freeman 1982; Skottun et al. 1987), whereas circular variance does not (Alitto and Usrey 2004), so we will begin by examining the first two measures and then consider the third.

For weak or balanced inhibition, the σ of the firing-rate tuning curves show no systematic variation with stimulus contrast for contrasts $\gtrsim$4%, whereas for strong inhibition, σ develops a small, but significant narrowing with increasing contrast (Fig. 5*A*, *left*). The HWHM data show a marked iceberg effect for weak *w*; contrast invariance is seen for balanced inhibition and strong inhibition yields, again, a small but significant negative trend with increasing contrast. Results for lower contrasts become extremely noisy, particularly with weak inhibition, making width difficult to measure and resulting in tuning that appears flat by our assay (σ or HWHM of 90°). Experimental data show at least approximate contrast invariance down to contrasts as low as 2% (Skottun et al. 1987); possible reasons for this discrepancy are addressed in the DISCUSSION.

To quantitatively assess the degree of contrast invariance, we assess the slope of the curve of width versus log contrast. The slope detects any trend in the data, such as an overall

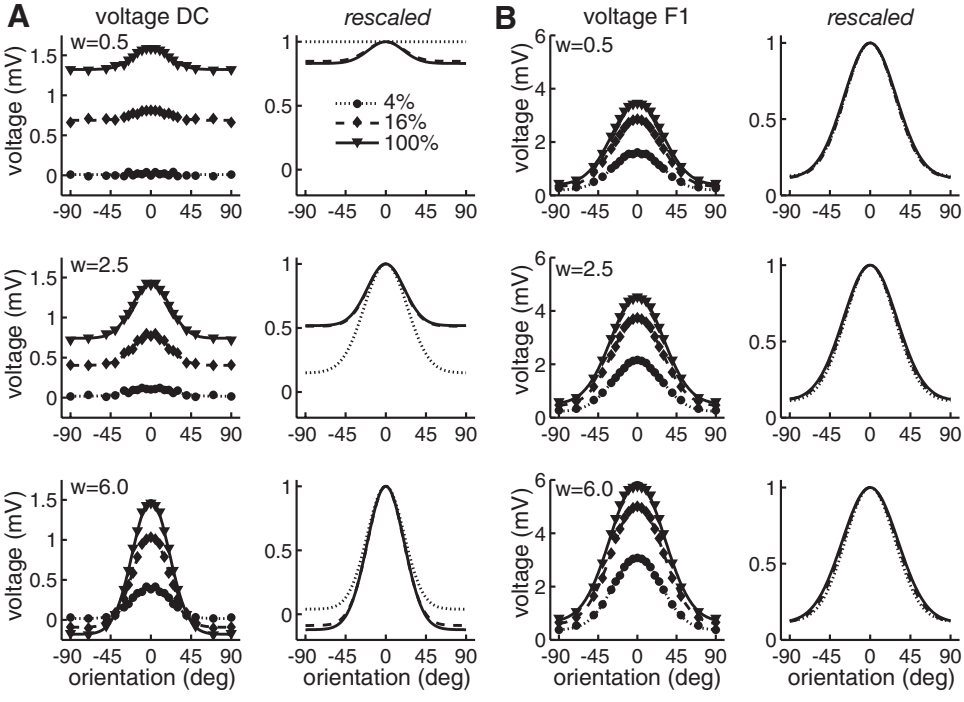

FIG. 4. Separate voltage tuning curves for the DC and F1 of the membrane potential. Data are plotted with the same format as in Fig. 3. DC voltage is measured relative to the resting membrane potential. *A*: mean, or DC, voltage tuning curves as a function of orientation at 3 contrasts (4, 16, and 100%) plotted for each of 3 values of *w*. From *top* to *bottom*: *w* increases from 0.5 to 6.0 as labeled. On the *right*, curves are normalized so that peaks coincide at 1 and 0 marks the resting membrane potential. *B*: same format as in *A*, but for the modulation, or F1, of the voltage. In the rescaled plots, 1 is where all peaks coincide and 0 is simply zero voltage.

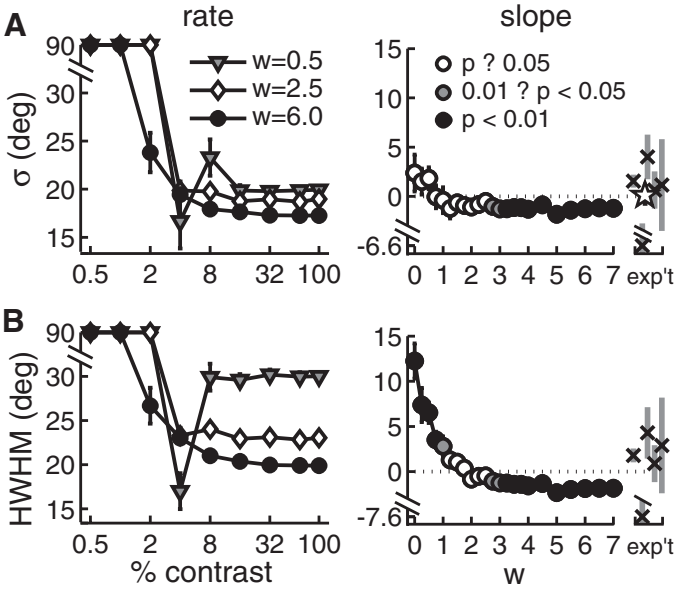

FIG. 5. Measures of the width and contrast invariance of the width of the rate tuning curves. *A*: σ of the Gaussian part of the fitted curves is plotted vs. $\log_{10}$ (*contrast*) in the *left panel*. A width of 90° indicates flat tuning. Slopes of these width curves for contrasts of ≥4° are plotted in the *right panel* vs. *w*, the inhibitory gain factor. Slope is measured in units of degrees per decade $\log_{10}$ (*contrast*). A value of 1 in these plots indicates a change of 1° over a contrast change from 10 to 100%. Shading of the points represents how significantly the measured mean deviates from zero as measured by a *t*-test. White circles indicate a value of $P \geq 0.05$; gray indicates $0.05 > P \geq 0.01$; black indicates a value of $P < 0.01$. Error bars on model data denote SE. Results from some experimental data are shown at the *right* of these model data. Black × symbols denote data from 5 cells from cat primary visual cortex (V1) measured intracellularly by J. Anderson and D. Ferster. Gray error bars here indicate SD. (Off-axis experimental data point is −6.573 ± 4.428, mean ± SD.) Star indicates the mean slope for data of Alitto and Usrey (2004) from V1 in ferrets with error bars indicating SE. *B*: HWHM is plotted vs. $\log_{10}$ (*contrast*). Same symbols are used as in *A*. HWHM is measured relative to the background firing rate. (Off-axis experimental data point in the *right panel* is −7.574 ± 5.006.) We label tuning as flat when less than one third of the 50 experiments revealed measurable tuning.

broadening of width with contrast. We measure the slope of tuning curves over contrasts of ≥4% because 4% is the lowest contrast at which we can reliably measure tuning for all values of *w*. In the firing rate data from the model, the slope of either σ or HWHM is not significantly different from zero for *w* in the range 1 to 3 and, in some cases, for smaller *w* [i.e., for weak to balanced inhibition (Fig. 5, *right*)]. For weaker inhibition, tuning broadens with increasing contrast (an iceberg effect), whereas for stronger inhibition, there is a small but significant trend for tuning to sharpen with increasing contrast. Data from a few cells ($n = 5$) measured intracellularly in cat V1 show variability in these measures greater than that seen in the model (slope in Fig. 5), but a larger sample of extracellularly recorded cells in ferret visual cortex ($n = 47$) shows a mean σ slope fairly tightly bounded at zero (star in Fig. 5*A*, *right*).

The DC voltage acquires a tuned component that evolves with increasing *w* as is shown in Fig. 6, *A* and *B*. Slopes of the DC voltage tuning are taken for contrast of ≥8% because this is the lowest contrast at which nonflat tuning is observed for most values of *w*. This tuning arises at lower contrasts for increasing *w*. The slope of the σ of the tuning is quite variable below about $w \cong 2.0$, where the tuning is noisy. Above $w \cong 2.0$ the slope is not significantly different from zero (Fig. 6*A*). For all *w*, the slope of the σ part of the DC tuning falls within the broad range of values observed experimentally in the five cells recorded by Anderson and Ferster. The HWHM of the DC grows with contrast at low *w* (Fig. 6*B*) as the result of a rising untuned component of the mean voltage. Above $w \cong 3.0$, this is sufficiently suppressed and the slope of the HWHM falls within the range of smaller slopes observed in three of the five intracellularly recorded cells.

Examining the tuning of F1 of the voltage (Fig. 6*C*) reveals some broadening. For all *w*, the F1 has a positive, though small, slope. This slope is, in part, attributed to the flattening of the peak in F1 tuning that results from the fixed spike threshold and reset in our model. If spiking is eliminated, which might better model the real data in which spike threshold is highly variable and there is little reset, the σ part of the fit to the voltage F1 becomes quite contrast invariant over all *w* (data not

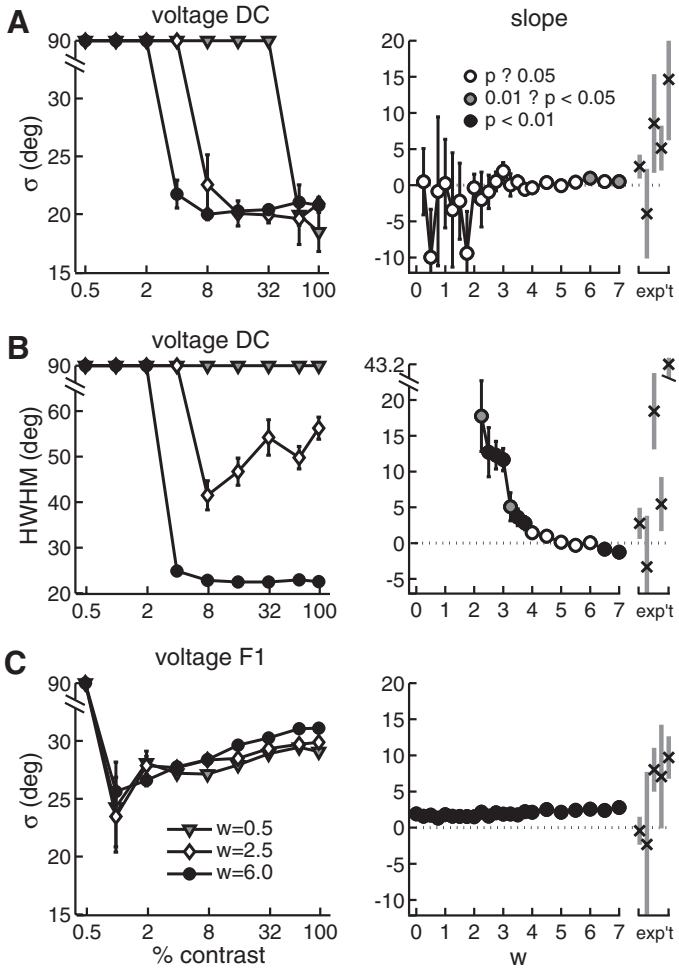

FIG. 6. Widths of DC and F1 voltage tuning curves and the slope of these widths vs. $\log_{10}$ (*contrast*). Slopes are measured in units of degrees per decade $\log_{10}$ (*contrast*). *A*: data are plotted as in Fig. 5 for the width and slope of the DC membrane potential. Width is plotted only for those data in which more than one third of the experiments gave nonflat tuning. Note that the DC acquires tuning only across many contrasts for higher values of *w*. Slope reflects that the Gaussian part of this tuning at contrasts of ≥8% is contrast invariant over a large range of *w*. *B*: same as in *A*, but for the HWHM of the voltage DC tuning. *x*-axis values without data points indicate that none of the 50 experiments showed nonflat tuning down to 8%. (Off-axis Ferster data point is 43.249 ± 14.717.) *C*: same format as in *A*, but for the F1 of the voltage, and with slopes measured for contrasts ≥4%.

shown). Experimentally observed slopes in this quantity vary widely and our model slopes fall within this range.

Suppression of the null

We have discussed the suppression of the untuned mean input in the rate and voltage responses and have attributed this suppression to inhibition. To make these statements more quantitative, we examine the variation of the rate and voltage responses at the null, defined as the orientation perpendicular to the preferred. The null rate increases with contrast at low w, has zero slope versus contrast for $3.0 \leq w \leq 3.75$, and decreases with contrast for higher w (Fig. 7*A*). Apart from one cell with a large positive slope, the in vivo intracellular data show a zero or slightly negative slope in the null rate (Fig. 7*A*). In extracellular recordings in ferret there was no significant change on average between null responses at low contrast and at high contrast (Alitto and Usrey 2004), although there was a statistically insignificant change in the mean null response corresponding to a slope of about −0.2 in Fig. 7*A*.

The inhibitory strength that achieves zero slope in the null rate depends on several factors. It is not necessary that the inhibition be strong enough to prevent depolarization by a null stimulus. On the contrary, a null stimulus induces a net depolarization that grows with contrast for all but the strongest inhibition (Fig. 7*B*). This is expected, given that our definition of "balanced" inhibition means that the inhibitory and excitatory currents balance at threshold voltage and so are depolarizing at rest voltage. Rather, to achieve a zero slope in the null rate, inhibition must be strong enough to keep the growing depolarization small enough that its effect on firing rate is negligible. This probably occurs through a combination of two effects. First, the power law function determining the firing rate as a function of voltage remains effectively zero for small enough depolarizations. Second, the increase in depolarization with contrast is accompanied by an increase in conductance that, assuming inhibition is stronger than balanced, has a subthreshold net reversal potential. This suppresses the probability of suprathreshold voltage fluctuations, offsetting the increasing depolarization. As an example, in our data for $w = 4.0$, the peak (F1 + DC) trial-averaged voltage at the null varies from 0.3 mV at 4% contrast to 1 mV at 100% contrast, whereas the RMS of voltage fluctuations shrinks from 3.5 mV at 4% contrast to 3.25 mV at 100% contrast. Thus the distance from peak trial-averaged voltage to threshold remains a constant number of SDs of the voltage noise across contrasts [(9.7/3.5) = 2.77 SDs at low contrast, (9/3.25) = 2.77 SDs at high contrast], suggesting a zero slope for firing rate. The slope is actually slightly negative for $w = 4.0$, suggesting some additional slight suppression of the high end of the voltage noise distribution with contrast, and indeed we also find that the kurtosis of the $w = 4.0$ voltage distribution decreases with contrast.

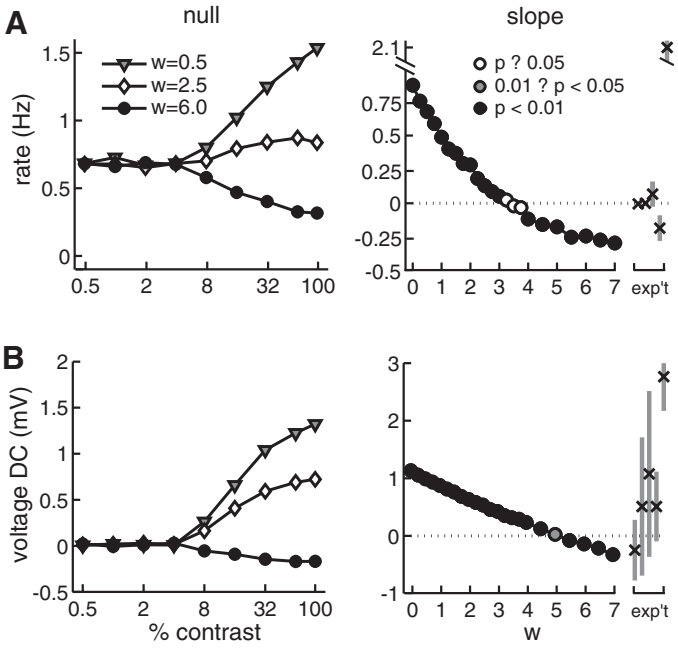

FIG. 7. Enhancement or suppression of the null rate and DC voltage as a function of contrast and w. *A*: average rate in response to a stimulus oriented at 90° relative to the preferred (the null) is plotted vs. $\log_{10}$ (*contrast*) for 3 values of the inhibitory gain w. Note that the null rate grows with increasing contrast for low w and passes monotonically, with increasing w, into a regime in which it is suppressed with increasing contrast. Slope of the rate for contrast ≥8% is shown in the *right panel*. Slope is measured in units of Hertz per decade $\log_{10}$ (*contrast*). Experimental data from Anderson and Ferster are shown for comparison. (Off-axis experimental data point is 2.106 ± 0.547.) One cell (the second one plotted from the *left*) had no null firing, whereas another (the *leftmost*) had a very low null firing rate. *B*: DC part of the voltage response to a null stimulus rises with contrast for all but the largest w. Curves are plotted as in *A*. Colors indicate significance of the slope as in previous plots and error bars indicate SE. Slopes are measured in units of millivolts per decade $\log_{10}$ (*contrast*).

Another indication of the presence of inhibition in physiological data is that the firing rate to a null stimulus at all measured contrasts tends to be lower than the background firing rate, both in the extracellular data of Alitto and Usrey (2004) and in the intracellular data from Anderson and Ferster. In the latter data, three of five cells showed suppression of the null firing at all contrasts, relative to the blank stimulus. In one remaining cell, null firing was suppressed at two of three contrasts tested, and in the other, null firing was higher at all contrasts than background. In the model, the null firing is suppressed relative to background for all contrasts that elicit a response when inhibition is strong enough to yield a negative slope in Fig. 7*A* (i.e., for $w \geq 3.5$).

Null/preferred ratio and circular variance are not contrast invariant

The extracellular studies of Alitto and Usrey (2004) also reported that the ratio of null to preferred orientation firing rates decreases with increasing contrast, with a slope of about −0.1 (a decrease of ratio from 0.14 to 0.08 over about 0.6 $\log_{10}$ units). Similar slopes in the range 0 to −0.1 are seen in four of the five cells measured intracellularly in vivo (Fig. 8*A*). A roughly similar decrease is seen in the model for all w, although strong inhibition is needed to make the slope as small as −0.1 (Fig. 8*A*). However, this slope depends on the starting point (i.e., the choice of low contrast), which was rather high in the extracellular recordings (average 21% contrast); using such a high starting point would give appropriately low slopes in the model for almost any w (e.g., when we measure the slope from 21 to 100%, the slope varies from −0.15 to −0.05 as w varies from 0.5 to 6.5). A negative slope is expected for many reasons: the power-law input–output relation between the

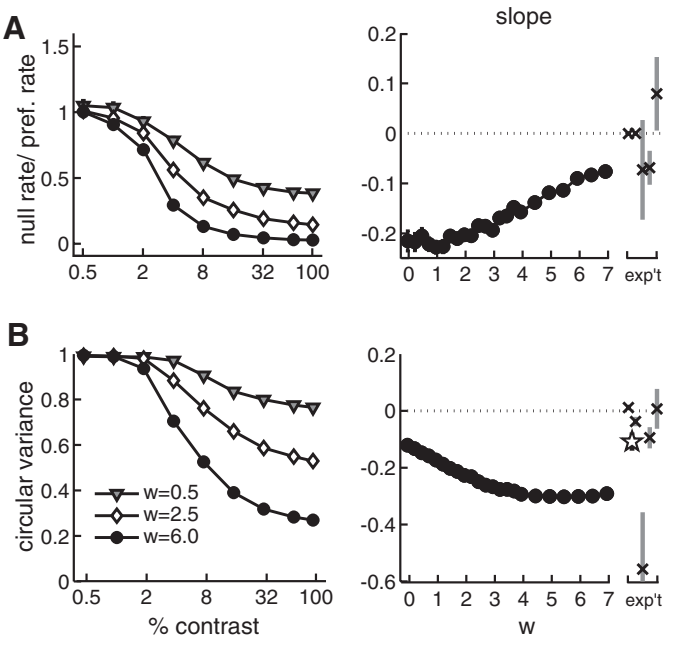

FIG. 8. Circular variance of the rate is not contrast invariant. *A*: null response rate divided by the preferred orientation response rate is plotted vs. $\log_{10}$ (*contrast*) in the *left panel*. Null rate is always suppressed relative to the preferred by increasing contrast. *B*: circular variance of the rate is plotted vs. $\log_{10}$ (*contrast*) for 3 values of *w*. These curves are not flat over any range of contrasts. Slopes of these curves over contrasts ≥4% are shown on the *right*. Slopes are measured in units of circular variance per decade $\log_{10}$ (*contrast*). Experimental data are plotted from the Ferster and Usrey groups as in Fig. 5 and show a trend toward negative slopes in the circular variance as do our model data. Usrey data (star) shows the slope from 21 to 100% contrast; model slopes are >4 to 100% contrast, but would be smaller if plotted over the 21–100% range; see RESULTS.

voltage and rate ensures that the null/preferred response ratio decreases with increasing contrast, and this is reinforced by the amplification of preferred but not null responses by recurrence and by the suppression of null but not preferred responses by inhibition (although complex-cell inhibition can also suppress preferred responses).

Another measure of width used by experimenters is the circular variance (Alitto and Usrey 2004; Ringach et al. 2002). This measure is sensitive to either a broader peak or a higher baseline in the orientation tuning curve—either increases the circular variance. In particular, for tuning curves that are well described as a Gaussian plus a baseline and for which the Gaussian tuning is invariant with stimulus contrast, both of which apply well to V1 cells, the circular variance increases monotonically with the ratio of the null to preferred response (see APPENDIX). This behavior is quite different from measures like σ, which are explicitly invariant with respect to changes in this ratio. Corresponding to the decrease of the null/preferred response ratio with contrast for all *w* (Fig. 8*A*), the circular variance of the firing rate response decreases with contrast over the entire range of *w* studied (Fig. 8*B*). Such a decrease was observed in extracellular recording by Alitto and Usrey (2004). The mean slope of this decrease was less in the extracellular recording (star in Fig. 8*B*, *right*) than that in the model, but again, slopes in the extracellular recording were measured starting from a low contrast that averaged 21%, whereas model slopes were calculated starting from 4% contrast. As can be roughly seen in Fig. 8*B*, *left*, model slopes would range from −0.08 to −0.13 as *w* varies from 0.5 to 6.5 if the larger values were used for the starting contrast. The in vivo intracellular data generally show negative slopes, but smaller than the mean of the extracellular recordings.

Complex-cell inhibition

We also tested the model with inhibition arising solely from complex inhibitory cells like those observed in Hirsch et al. (2003) and modeled in Lauritzen and Miller (2001). Those cells had overlapping light and dark responses throughout their receptive fields and were essentially untuned for orientation. We model input from these cells in response to gratings of any orientation as temporally unmodulated and growing with contrast: $g^I_{FF,complex} = wg_{stim}DC(C)$. This inhibition suppresses the untuned DC excitation without affecting the F1. Thus an increase in *w* now suppresses firing to all stimulus orientations, whereas with simple-cell–like inhibition, the inhibition induced an increase in input F1 that compensated for the decrease in input DC at preferred orientations. To adjust for this difference, we increased the stimulus amplitude and modified the background conductances to maintain a nonzero background firing rate ≲1 Hz. Parameters were set as detailed in METHODS.

With complex-cell inhibition, contrast invariance of the rate can be achieved for low *w* (Fig. 9, *A* and *B*). With weak inhibition, both the σ and the HWHM of the rate are approximately contrast invariant. With balanced or strong inhibition, the tuning narrows with increasing contrast, as is particularly evident in the HWHM. Thus for weak inhibition, we can achieve contrast invariance of the firing rate in our model cell with complex-cell–like inhibition.

We cannot, however, realistically suppress the null response (Fig. 9*C*) with such weak inhibition. In response to a null-oriented stimulus, the rate response (Fig. 9*C*) and the voltage response (Fig. 9*F*) behave very much as in the case of simple-cell inhibition (Fig. 7, *A* and *B*), except that the absolute values of slopes are now larger because the model LGN input is stronger. This is as expected because, in response to a null stimulus, the simple-cell inhibition provides only a DC and thus is identical to the complex-cell inhibition. In particular, inhibition must be slightly stronger than excitation to prevent null firing from increasing with contrast.

We cannot achieve a tuned DC potential (Fig. 9, *D* and *E*) for any level of inhibition. For low levels of inhibition, the σ part of the voltage DC shows roughly contrast-invariant tuning for contrasts of ≥16% (at lower contrasts, we do not pull out any peaks from the noise), but by the HWHM measure, the voltage DC is never tuned for orientation. For weak inhibition, the untuned DC dominates the tuned DC just as for simple-cell inhibition. Stronger inhibition suppresses the growth of the untuned DC (and thus suppresses the growth of null responses), but the strong complex-cell inhibition also sufficiently suppresses the rate in response to preferred orientations such that the recurrent connections no longer induce an appreciable mean depolarization at those orientations. Thus little or no tuned DC is created, so that the tuned component of the DC remains smaller than the untuned DC component for all inhibition levels.

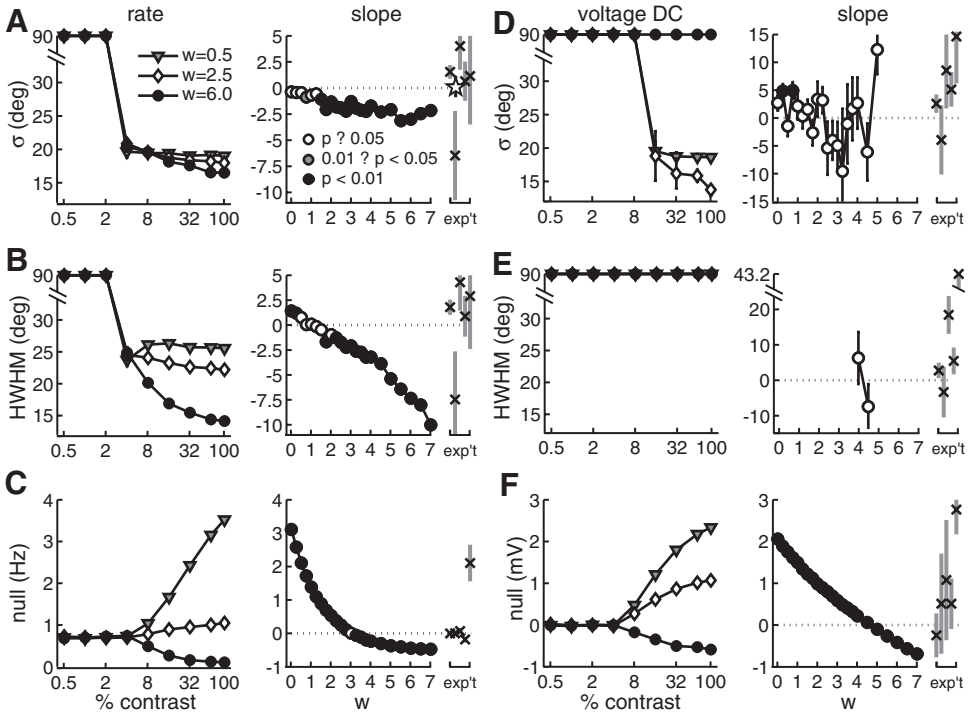

FIG. 9. Summary data from a model with complex-cell–like inhibition reveal that contrast invariance can be obtained in rate tuning but not in the DC potential. *A*: tuning of the σ from the fit of a Gaussian-plus-background to the rate tuning curve as a function of $\log_{10}$ (*contrast*), and the slope of these curves vs. *w*. Slope of the rate is close to zero for lower values of *w*. *B*: similar plots as in *A*, but for the HWHM of the firing rate. *C*: null rate is suppressed at high values of *w*, as shown here as a function of contrast (*left*) and as the slope for each *w* (*right*). High values of *w* are needed to give the null a negative slope. *D*: σ of the DC voltage reveals a tuned DC for small values of *w* that is suppressed at higher values of *w*. *E*: HWHM of the DC voltage tuning is flat for all *w*. *F*: null DC voltage shows suppression only at high values of *w*. Symbol conventions are as used in previous figures. All model data are shown with error bars indicating SE. All slopes except in *D* and *E* are measured for contrasts of ≥4%. In *D* and *E*, slopes were taken for contrasts of ≥16%. Where slope data are not plotted, none of the 50 experiments showed nonflat tuning down to 16% contrast; 2 data points in the plot of the slope in *E* show very noisy tuning and reflect data from a small number of model experiments (<10 of 50) where tuning was not flat. All Anderson and Ferster data are reported as before, using crosses and showing gray bars indicating the SD about the mean. Data from Alitto and Usrey (2004) are plotted in *A* with a star and with error bars indicating the SE. Slopes in *A*, *B*, *D*, and *E* are measured in units of degrees per decade $\log_{10}$ (*contrast*), slopes in *C* in units of Hertz per decade $\log_{10}$ (*contrast*), and slopes in *F* in units of millivolts per decade $\log_{10}$ (*contrast*).

DISCUSSION

We have found that, given realistic voltage noise, both the contrast invariance of orientation tuning (Alitto and Usrey 2004; Anderson et al. 2000a; Sclar and Freeman 1982; Skottun et al. 1987) and the decrease with contrast of circular variance (Alitto and Usrey 2004) of spiking responses are easily attained, by levels of feedforward inhibition ranging from weak to strong. The reasons are much as illustrated in the *right column* of Fig. 1*B*: the power-law input–output relation induced by the voltage noise strongly amplifies larger inputs relative to smaller inputs. This ensures that the main tuning peak is largely determined by the F1 of the input, which is contrast invariant, almost irrespective of inhibition levels. However, proper suppression of the input DC is also required: if inhibition, and thus DC suppression, is very weak, a weak broadening of tuning with contrast occurs, whereas if inhibition is too strong, a weak narrowing occurs (Fig. 5). The power law also ensures that the ratio of null-orientation to preferred-orientation spiking responses decreases with increasing contrast, which is reinforced by the amplification of preferred but not null responses by recurrence and the inhibition of null but not preferred responses by antiphase inhibition. This in turn ensures (see APPENDIX) that the circular variance decreases with contrast (Fig. 8).

Although the contrast invariance of spike-rate tuning does not place significant constraints on the strength of inhibition, stronger constraints arise from two observations. First, the voltage DC shows contrast-invariant orientation tuning. This requires inhibition to be stronger than excitation (Fig. 6*B*), so that the untuned voltage DC induced by the LGN input is sufficiently suppressed relative to the tuned voltage DC induced by recurrent excitation. However, the constraints from experimental data on the contrast invariance of the voltage DC are not strong (Fig. 6*B*). Furthermore, to the extent that LGN input is weaker and recurrent excitation is stronger than those in our model (as discussed in the following text), the ratio of tuned to untuned DC component will increase and so the requirement for inhibition may correspondingly decrease. The observation of a tuned, contrast-invariant voltage DC also seems to require antiphase inhibition, which allows suppression of null voltage responses without corresponding suppression of preferred responses, and does not appear to be achievable with phase-nonspecific complex cell inhibition alone.

A second constraint on inhibition arises from the spiking response to a null-oriented stimulus, which on average does not grow with contrast and is smaller than background firing (Alitto and Usrey 2004 and intracellular data from Anderson and Ferster); however, it will be important to measure this in cells known to receive strong LGN input). In our model, this

again requires inhibition to be slightly stronger than excitation (Figs. 7*A* and 9*C*). Two effects are involved. The null stimulus evokes an average depolarization that grows with contrast (unless inhibition is extremely strong), and evokes a conductance increase that grows with contrast that depresses the probability of large voltage fluctuations. The stronger the inhibition, the smaller the depolarization and the larger the conductance change. To match the data, inhibition must be strong enough that there is no net increase with contrast in the probability of a suprathreshold voltage fluctuation. In general, this seems to require inhibition that is stronger than excitation. However, the further the distance from rest to threshold or the weaker the overall LGN input, the wider the range of inhibitory strengths that will produce slopes of null firing versus contrast indistinguishable from zero. This constraint also provides an argument that antiphase inhibition must supplement phase-nonspecific complex-cell inhibition: we have found that, if inhibition comes only from complex cells, then inhibition that is strong enough to suppresses spiking to a null stimulus despite voltage fluctuations also causes narrowing of orientation tuning with contrast.

An additional argument that inhibition is needed to suppress spiking to a null stimulus is that the peak LGN input is higher to a high-contrast null stimulus than to a low-contrast preferred stimulus (see Troyer et al. 1998). For the latter and not the former to induce spiking, either the null input must be reduced by inhibition, and/or the size of fluctuations that might carry the null input over threshold must be relatively reduced, which in our model occurs primarily as a result of the conductance added by inhibition.

Critique of our model

Our model has certain limitations. The recurrent excitation is necessarily weak because of our simplified model of recurrence: only a single cell gives recurrent input. This leads to instability at lower values of the overall amplification than can be achieved in more realistic models in which recurrence is distributed over hundreds or thousands of inputs. In our model, the voltage F1 is amplified about 1.5-fold relative to that induced by the LGN alone, for simple-cell inhibition with $w = 2.5$. About 85% of this model amplification arises from the antiphase inhibition rather than recurrent excitation, so the amplification is correspondingly reduced for smaller w and increased for larger w. This amplification is weaker than the rough experimental estimate that the voltage F1 is typically amplified two- to threefold (Ferster et al. 1996), although work published after ours was completed documents that simple cells show great variety in their relative strength of LGN versus intracortical input (Finn et al. 2007).

Another possible limitation concerns the voltage distance from rest to threshold. We assumed a distance of 10 mV, which roughly described the five sample cells we studied from Anderson and Ferster (mean 13 mV, range 8–20 mV). However, a more recent study with far more cells found an average distance from rest to threshold of 19.8 mV for simple cells (Priebe et al. 2004). An increased distance from rest to threshold would increase the range of depolarizations that yield effectively zero increase in firing rate for a given voltage noise level (i.e., the range over which the resulting increase in average firing rate is smaller than experiment can resolve), whereas a weaker ratio of LGN input to intracortical input would help keep depolarizations in response to a null stimulus within this range. Thus either change might increase the range of w that effectively give zero slopes in the tuning width and the null firing rate as functions of contrast.

We have estimated the DC/F1 ratio of the LGN input assuming a Gabor function receptive field. The actual arrangement of LGN input is likely to be a quite noisy version of the Gabor function (Alonso et al. 2001), and this noise would significantly increase the DC relative to the F1. Thus we have probably underestimated the relative size of the input DC.

All of these factors may contribute to another limitation: that the model DC/F1 ratio for voltage response to preferred orientation stimuli is smaller than that observed in intracellular recordings. In our model the DC varies roughly from 15 to 30% of the F1 as contrast varies (see METHODS). In the five experimental cells from Anderson and Ferster the ratio ranges between 2 and 2.5. More recent data including many more cells Priebe et al. (2004) show that, at high contrast, voltage DC/F1 ratios of $\lesssim$0.8 (and ranging to $\leq$0.4) are seen only among the cells with the highest F1/DC ratio of spike rate responses (which one might speculate are most likely to include simple cells receiving strong LGN input, as modeled here). Thus the degree of discrepancy is unclear, but there is a discrepancy.

To summarize, in our model as it stands, we observe that stronger than balanced feedforward inhibition is needed to suppress firing responses to a null stimulus and to achieve proper tuning of the voltage DC. Weaker inhibition might be able to satisfy these constraints, however, if some combination of weaker LGN input and/or a larger distance from rest to threshold were instantiated in the model. These remain open issues for future study. In addition, antiphase inhibition is needed to satisfy these constraints. These results differ from those of our previous work, which did not incorporate voltage noise: in those studies, stronger than balanced inhibition was required to attain contrast invariance of spike-rate tuning (Troyer et al. 1998) and complex-cell inhibition was sufficient by itself to achieve this (Lauritzen and Miller 2003). Thus the key issues to be addressed to determine the size and structure of feedforward inhibition are substantially changed by the effects of voltage noise.

Since this work was completed, we became aware of results showing that a decrease in noise level with contrast makes an important contribution to contrast-invariant orientation selectivity, allowing larger depolarizations to high-contrast null stimuli without increases in null spiking (Finn et al. 2007). Although such effects occurred in our simulations and contributed to our results, we assumed from the contrary results of Anderson et al. (2000a), who saw little dependency of noise level on orientation or contrast, that these effects played a relatively minor role, and we chose our parameter regimes accordingly. Further work will be needed to determine how these results—and also the results in the same paper on the variation across simple cells of the percentage of input received from LGN and the covariation of this with response properties such as the tuning of the voltage DC—influence the conclusions as to the strength of inhibition required to explain spiking and voltage tuning.

Comparison to other models

In the model we study here, spiking response properties emerge from the combination of feedforward input, both excitatory and inhibitory, and the nonlinearity of spike threshold, which along with voltage noise creates a power-law input–output function. Recurrent intracortical excitation amplifies but does not create spiking response properties; however, it is important for explaining voltage response properties, such as the tuned voltage DC. Previous models (Ben-Yishai et al. 1995; Somers et al. 1995) explained the contrast invariance of spiking orientation tuning as a result of intracortical connections that cause any stimulus to yield a "bump" of cortical activity of a fixed width. As we have discussed previously (Troyer et al. 1998), this is inconsistent with the fact that orientation tuning width does depend on stimulus attributes, such as length of a bar or spatial frequency of a grating, even though it does not depend on the stimulus attribute of contrast. It also seems incompatible with experiments showing similar voltage orientation tuning with or without cortical connections (Chung and Ferster 1998; Ferster et al. 1996). Another model (McLaughlin et al. 2000; Wielaard et al. 2001) is similar to that of Troyer et al. (1998) in that spiking response properties are explained by strong untuned inhibition that eliminates the untuned, nonlinear component of the LGN excitatory input. However, this model uses only phase-nonspecific intracortical connections. In such a model, cortical connections do not amplify the voltage F1, unlike in experiments (Ferster et al. 1996), and the inhibitory conductance has no F1 at all, which again differs from experiment (Anderson et al. 2000b; Priebe and Ferster 2006). It would also be difficult or impossible to construct simple cells that receive a significant percentage of their excitation from cortex, as observed recently (Finn et al. 2007), without phase-specific excitation, or to build simple cells in which the orientation tuning of the inhibitory conductance is strongly peaked at the cell's preferred orientation, as typically observed for simple cells (Anderson et al. 2000b; Ferster 1986; Martinez et al. 2002), without antiphase inhibition.

Experimental implications

Direct measurements of inhibitory and excitatory conductance to a null stimulus in cells receiving strong LGN input could most cleanly determine the strength of inhibition. Existing measurements for seven simple cells suggest that most have stimulus-induced inhibitory conductance at the null comparable in size to stimulus-induced excitatory conductance (Anderson et al. 2000b), which represents weak ($w \approx 1.0$) rather than balanced ($w \approx 2.5$) inhibition. However, LGN input to these cells was not assessed.

Experimental data are highly variable. One source of this variation might be variability in the strength of inhibition received by cells relative to excitation. If so, measures of tuning widths and null suppression of spiking and voltage responses should show covariation, on average, as they do if w is varied in the model. For example, cells that show a negative slope in the rate tuning width as a function of contrast should also tend to show a negative slope in the null firing. This provides one interesting set of experimental tests of the present results.

We observed contrast-invariant rate tuning down to about 4% contrast. Experimentally, this is seen to about 2% contrast, at least in some cells (Skottun et al. 1987). Possible explanations are that our model of LGN contrast response may be inaccurate at very low contrasts [it was derived from data of Cheng et al. (1995), who did not examine such low contrasts], or that cells that respond to such low contrasts may receive stronger LGN synapses than do model cells. An alternative explanation begins by noting that, in model data, the voltage responses for balanced or dominant inhibition are contrast invariant down to 1 or 2% contrast (data not shown). Thus the problem may be a failure to create spike responses from these small but tuned voltage responses. A larger tuned DC voltage response might help to cure this.

To account for the observed orientation tuning of the voltage DC, the tuned component of the voltage DC must be large relative to the untuned component. The LGN input has only an untuned DC, so the tuned component is created in cortex. There are two obvious mechanisms to create this component: recurrent excitation, which creates a component with tuning that should roughly follow spiking tuning; and reversal potential effects allowing voltage modulations from rest to go up more strongly than they can go down, which should create tuning that roughly follows voltage F1 tuning. Comparing the tuning width of the voltage DC to that of spiking and the voltage F1 may be one way to assess how much each effect contributes.

We have considered two components of feedforward inhibition: an F1 component that is opposite in phase to feedforward excitation and a DC component. We have equated the combination of an F1 and a DC with antiphase inhibition from inhibitory simple cells that have both an orientation-tuned and an untuned component to their spiking response, as in Troyer et al. (1998, 2002). Hirsch et al. (2003) found a minority of inhibitory simple cells in layer 4 of cat V1 with such an untuned component, but the majority showed only a tuned component. We have equated inhibition consisting only of a DC component with inhibition from complex inhibitory cells, which show both light and dark responses throughout their receptive field and show little or no orientation tuning (Hirsch et al. 2003).

In reality, the inhibition received by simple cells probably includes both simple- and complex-cell inhibition. Simple cells without an untuned response component would provide a tuned F1 and, if their mean firing rate increased in response to a stimulus, a tuned DC. Simple cells with an untuned component would provide a tuned F1, an untuned DC, and perhaps a tuned DC component (if their mean firing rate did not increase equally at all orientations). The complex cells would provide an untuned DC. The net result would be much as in our simple-cell model, but with two possible changes: *1*) changes in the relative strength of the inhibitory F1 and inhibitory untuned DC and *2*) the possible addition of a tuned inhibitory DC. Neither of these seems likely to seriously change our analysis, so that we believe our "simple-inhibitory-cell" case can really be understood as a mixture of simple and complex inhibitory cells.

The fluctuation-driven regime and functional specificity

The present model accounts for responses in a regime in which the trial-averaged or mean voltage response is subthreshold and spiking is driven by voltage fluctuations (Ander-

son et al. 2000a). Our previous models had little voltage noise, so that spiking was driven primarily by the mean voltage response. Orientation tuning is created differently in these two regimes (Fig. 1*B*). When firing on the fluctuations, the mean voltage response is put through a power law to create the spiking response, narrowing the tuning without a hard threshold. The spiking tuning then is contrast invariant if the voltage tuning is. When firing on the mean, the tuning is determined by the range of orientations that drive a suprathreshold voltage response. Contrast-invariant spiking tuning then requires inhibition that is stronger than excitation.

These two regimes require very different settings of the distance from rest to threshold relative to the size of the mean voltage responses. Fortunately, in both regimes the settings seem to arise naturally. A key constraint is that the spontaneous activity of the simple cells should be small (<1 Hz) but not zero. In the noise-driven regime, this ensures that rest is far enough from threshold, relative to noise fluctuations, that the trial-averaged stimulus-driven voltage responses are likely to stay subthreshold (although other constraints on stimulus-driven responses also contribute). In the mean-response–driven regime, this similarly ensures that rest is close enough to threshold that stimulus-driven responses are likely to be suprathreshold.

One could imagine exploring intermediate levels of noise. So long as responses stayed clearly in one regime or the other, we expect little change in the analysis. However, if the two regimes were straddled, low-contrast responses would fire on fluctuations whereas high-contrast responses would fire on the mean. This would likely lead to different tuning widths in the two regimes absent careful parameter adjustment.

Large voltage noise is seen in many (e.g., Destexhe et al. 2003), although perhaps not all (e.g., Deweese and Zador 2004), cortical systems. The results presented here, by identifying specific ways in which voltage noise and feedforward inhibition can interact to create stimulus specificity in the context of cat V1, may provide a first step toward understanding such cortical processing more generally.

APPENDIX

The circular variance is given by $1 - |\sum_i y(\theta_i)e^{i2\theta_i}/\sum_i y(\theta_i)|$, where we multiply the angle θ by a factor of 2 because orientation has π periodicity. For Gaussian tuning curves described by $y(\theta) = A\exp[-(\theta-\theta_0)^2/2\sigma^2] + B$, the circular variance has the form

Circular variance

$$= \frac{A\sum_i \exp[-(2\theta_i)^2/(2(2\sigma)^2)][1-\cos(2\theta_i)] + B\sum_i[1-\cos(2\theta_i)]}{A\sum_i \exp[-(2\theta_i)^2/(2(2\sigma)^2)] + N_\theta B}$$

where the i runs over all N_θ orientations and we have multiplied θ and σ by a factor of 2 once again to account for the π periodicity of orientation. Here, we have exploited the fact that the tuning is symmetric, which allows us to ignore the complex part of the circular variance. The responses at the null and preferred orientations can be related to the tuning parameters by $pref = A + B$ and $null = A\exp[-\pi^2/(2(2\sigma)^2)] + B$ or, equivalently, $A = (null - pref)/(\exp[-\pi^2/(2(2\sigma)^2)] - 1)$ and $B = pref - A$. Substituting these expressions into our equation for the circular variance and rearranging terms, and letting $G_\pi = \exp[-\pi^2/(2(2\sigma)^2)]$, $G_i = \exp[-(2\theta_i)^2/(2(2\sigma)^2)]$, and $\cos_i = \cos(2\theta_i)$, we obtain

$$\text{Circular variance} = \frac{a_1 + a_2\dfrac{null}{pref}}{a_3 + a_4\dfrac{null}{pref}} \quad (A1)$$

where

$$a_1 = N_\theta G_\pi - \sum_i G_i(1-\cos_i)$$

$$a_2 = \sum_i G_i(1-\cos_i) - N_\theta$$

$$a_3 = N_\theta G_\pi - \sum_i G_i$$

and

$$a_4 = \sum_i G_i - N_\theta$$

The extent to which any one set of a values can be used to fit the circular variance at all contrasts reveals how contrast invariant σ is. Alitto and Usrey (2004) found, for their data in the ferret visual cortex, that the circular variance varies as the square root of the null to preferred ratio. Given the form of the circular variance, it can masquerade as many different powers of the ratio of the null to preferred response, but we find that our data collapse to a line most precisely using the above function as a fit.

For tuning curves that are well described by a Gaussian plus a baseline, and for which the Gaussian tuning is invariant with stimulus contrast, the change in circular variance with a change in contrast can be determined as follows: Because the Gaussian tuning is contrast invariant, the parameters a_1, a_2, a_3, and a_4 do not vary with contrast. Thus by letting $x = null/pref$, we have

$$\frac{d\{circvar\}}{d\{contrast\}} = \frac{d\{circvar\}}{dx}\frac{dx}{d\{contrast\}}$$

and

$$\frac{d\{circvar\}}{dx} = \frac{a_2a_3 - a_1a_4}{(a_3 + a_4x)^2}$$

Thus the sign of $d\{circvar\}/dx$ is equal to the sign of $dx/d\{contrast\}$ times the sign of $(a_2a_3 - a_1a_4)$. The latter term is given by

$$a_2a_3 - a_1a_4 = N_\theta(1-G_\pi)\sum_i G_i\cos_i$$

This is always positive and becomes small relative to its peak value only for unrealistically large σ (empirically, $\sigma > 90°$), which makes both $(1 - G_\pi)$ and $\sum_i G_i\cos_i$ small, or unrealistically small σ (empirically, $\sigma < 4°$), which makes $\sum_i G_i\cos_i$ small. Thus the change in circular variance with contrast has the same sign as the change in *null/pref* with contrast: if the latter decreases with contrast, so will the circular variance.

ACKNOWLEDGMENTS

We thank the Ferster laboratory and, in particular, J. Anderson for access to the lab's raw data. We benefited from useful discussions with D. Ferster, D. McCormick, L. Osborne, N. Priebe, P. Sabes, and T. Troyer.

GRANTS

This work was funded, in part, by National Eye Institute Grant RO1-EY-11001. S. E. Palmer received support from the Sloan and Swartz foundations and from Novartis, through the Life Sciences Research Foundation.

REFERENCES

Alitto HJ, Usrey WM. Influence of contrast on orientation and temporal frequency tuning in ferret primate visual cortex. *J Neurophysiol* 91: 2797–2808, 2004.

Alonso JM, Usrey WM, Reid RC. Rules of connectivity between geniculate cells and simple cells in cat primary visual cortex. *J Neurosci* 21: 4002–4015, 2001.

Anderson JS, Carandini M, Ferster D. Orientation tuning of input conductance, excitation, and inhibition in cat primary visual cortex. *J Neurophysiol* 84: 909–926, 2000b.

Anderson JS, Lampl I, Gillespie D, Ferster D. The contribution of noise to contrast invariance of orientation tuning in cat visual cortex. *Science* 290: 1968–1972, 2000a.

Ben-Yishai R, Bar-Or RL, Sompolinsky H. Theory of orientation tuning in visual cortex. *Proc Natl Acad Sci USA* 92: 3844–3848, 1995.

Cheng H, Chino YM, Smith EL 3rd, Hamamoto J, Yoshida K. Transfer characteristics of lateral geniculate nucleus X neurons in the cat: effects of spatial frequency and contrast. *J Neurophysiol* 74: 2548–2557, 1995.

Chung S, Ferster D. Strength and orientation tuning of the thalamic input to simple cells revealed by electrically evoked cortical suppression. *Neuron* 20: 1177–1189, 1998.

Destexhe A, Rudolph M, Fellous J, Sejnowski T. Fluctuating synaptic conductances recreate in vivo-like activity in neocortical neurons. *Neuroscience* 107: 13–24, 2001.

Destexhe A, Rudolph M, Paré D. The high-conductance state of neocortical neurons in vivo. *Nat Rev Neurosci* 4: 739–751, 2003.

Deweese M, Zador A. Shared and private variability in the auditory cortex. *J Neurophysiol* 92: 1840–1855, 2004.

Ferster D. Orientation selectivity of synaptic potentials in neurons of cat primary visual cortex. *J Neurosci* 6: 1284–1301, 1986.

Ferster D, Chung S, Wheat H. Orientation selectivity of thalamic input to simple cells of cat visual cortex. *Nature* 380: 249–252, 1996.

Ferster D, Miller KD. Neural mechanisms of orientation selectivity in the visual cortex. *Ann Rev Neurosci* 23: 441–471, 2000.

Finn I, Priebe N, Ferster D. The emergence of contrast-invariant orientation tuning in simple cells of cat visual cortex. *Neuron* 54: 137–152, 2007.

Gillespie DT. The mathematics of Brownian motion and Johnson noise. *Am J Phys* 64: 225–240, 1996.

Hansel D, van Vreeswijk C. How noise contributes to contrast invariance of orientation tuning in cat visual cortex. *J Neurosci* 22: 5118–5128, 2002.

Hausser M, Roth A. Estimating the time course of the excitatory synaptic conductance in neocortical phyramidal cells using a novel voltage jump method. *J Neurosci* 17: 7606–7625, 1997.

Hestrin S. Different glutamate receptor channels mediate fast excitatory synaptic currents in inhibitory and excitatory cortical neurons. *Neuron* 11: 1083–1091, 1993.

Hestrin S, Nicoll RA, Perkel DJ, Sah P. Analysis of excitatory synaptic action in pyramidal cells using whole-cell recording from rat hippocampal slices. *J Physiol* 422: 203–225, 1990.

Hirsch JA, Martinez LM, Pillai C, Alonso JM, Wang Q, Sommer FT. Functionally distinct inhibitory neurons at the first stage of visual cortical processing. *Nat Neurosci* 6: 1300–1308, 2003.

Krukowski AE, Miller KD. Thalamocortical NMDA conductances and intracortical inhibition can explain cortical temporal tuning. *Nat Neurosci* 4: 424–430, 2001.

Lauritzen TZ, Miller KD. Different roles for simple-cell and complex-cell inhibition in V1. *J Neurosci* 23: 10201–10213, 2003.

Martinez L, Alonso J, Reid R, Hirsch J. Laminar processing of stimulus orientation in cat visual cortex. *J Physiol* 540: 321–333, 2002.

Martinez L, Wang Q, Reid R, Pillai C, Alonso J, Sommer F, Hirsch J. Receptive field structure varies with layer in the primary visual cortex. *Nat Neurosci* 8: 372–379, 2005.

McLaughlin D, Shapley R, Shelley M, Wielaard DJ. A neuronal network model of macaque primary visual cortex (V1): orientation selectivity and dynamics in the input layer 4cα. *Proc Natl Acad Sci USA* 97: 8087–8092, 2000.

Miller KD, Troyer TW. Neural noise can explain expansive, power-law nonlinearities in neural response functions. *J Neurophysiol* 87: 653–659, 2002.

Monier C, Chavane F, Baudot P, Graham L, Frégnac Y. Orientation and direction selectivity of synaptic inputs in visual cortical neurons: a diversity of combinations produces spike tuning. *Neuron* 37: 663–680, 2003.

Movshon JA, Thompson ID, Tolhurst DJ. Spatial and temporal contrast sensitivity of neurones in areas 17 and 18 of the cat visual cortex. *J Physiol* 283: 101–120, 1978.

Priebe N, Mechler F, Carandini M, Ferster D. The contribution of spike threshold to the dichotomy of cortical simple and complex cells. *Nat Neurosci* 7: 1113–1122, 2004.

Priebe NJ, Ferster D. Mechanisms underlying cross-orientation suppression in cat visual cortex. *Nat Neurosci* 9: 552–561, 2006.

Ringach D, Shapley R, Hawken M. Orientation selectivity in macaque v1: diversity and laminar dependence. *J Neurosci* 22: 5639–5651, 2002.

Sclar G, Freeman RD. Orientation selectivity in the cat's striate cortex is invariant with stimulus contrast. *Exp Brain Res* 46: 457–461, 1982.

Skottun BC, Bradley A, Sclar G, Ohzawa I, Freeman RD. The effects of contrast on visual orientation and spatial frequency discrimination: a comparison of single cells and behavior. *J Neurophysiol* 57: 773–786, 1987.

Somers D, Nelson SB, Sur M. An emergent model of orientation selectivity in cat visual cortical simple cells. *J Neurosci* 15: 5448–5465, 1995.

Stern P, Edwards FA, Sakmann B. Fast and slow components of unitary EPSCs on stellate cells elicited by focal stimulation in slices of rat visual cortex. *J Physiol* 449: 247–278, 1992.

Troyer TW, Krukowski AE, Miller KD. LGN input to simple cells and contrast-invariant orientation tuning: an analysis. *J Neurophysiol* 87: 2741–2752, 2002.

Troyer TW, Krukowski AE, Priebe NJ, Miller KD. Contrast-invariant orientation tuning in cat visual cortex: feedforward tuning and correlation-based intracortical connectivity. *J Neurosci* 18: 5908–5927, 1998.

Troyer TW, Miller KD. Physiological gain leads to high ISI variability in a simple model of a cortical regular spiking cell. *Neural Comput* 9: 971–983, 1997.

Wielaard DJ, Shelley M, McLaughlin D, Shapley R. How simple cells are made in a nonlinear network model of the visual cortex. *J Neurosci* 21: 5203–5211, 2001.